DOI:
10.1115/1.4054408

Document Version
Peer reviewed version

Journal of Mechanisms and Robotics. Received December 01, 2021;
Accepted manuscript posted April 17, 2022. doi:10.1115/1.4054408

Origaker: A Novel Multi-Mimicry Quadruped Robot Based on A Metamorphic Mechanism

Zhao Tang*
School of Mechanical Engineering
Tianjin University
Tianjin 300072, China
Email: zhaotang@tju.edu.cn

Kun Wang*
Centre for Robotics Research
Department of Engineering
King's College London
Strand, London WC2R 2LS, U.K.
Email: kun.3.wang@kcl.ac.uk

Emmanouil Spyrakos-Papastavridis
Centre for Robotics Research
Department of Engineering
King's College London
Strand, London WC2R 2LS, U.K.
Email: emmanouil.spyrakos@kcl.ac.uk

Jian S. Dai†
Professor, Fellow of ASME
Southern University of Science and Technology
Shenzhen, Guangdong, China;
Centre for Robotics Research
Department of Engineering
King's College London
Strand, London WC2R 2LS, U.K.
Email: jian.dai@kcl.ac.uk

This paper presents the Origaker, a novel multi-mimicry quadruped robot. Based on a single-loop spatial metamorphic mechanism, the Origaker is able to transform between different working modes, as the reptile-, arthropod-, and mammal-like modes, without disassembly and reassembly. The combination of the metamorphic mechanism and the quadruped robot enables the Origaker to pitch vertically, twist horizontally, and change the positional correlation between the trunk and legs. In consideration of its reconfigurability and structure adaptability, gaits and movement strategies, namely the fast spinning gait, the stair climbing gait, the self recovery, packaging, and crawling through narrow spaces and right-angled bends, were proposed and analyzed, demonstrating that the metamorphic mechanism provides the robot with enhanced locomotivity. Finally, a prototype was developed and experimentally tested. The experiment demonstrates that the robot can crawl over various surfaces, execute the designed gaits and strategies on different terrains, and conquer challenging obstacles.

*These authors contributed equally to this work.
†Corresponding author.

1 INTRODUCTION

In nature, locomotivity is of great importance for survival. Animals demonstrate excellent maneuverability when hunting or fleeing [1], especially legged mammals, reptiles, and arthropods. Apart from being paramount in nature, the locomotive ability of legged robots gives rise to considerable research interest because of the advantages that it offers over wheeled and tracked robots on rough terrains. In recent years, there are many advanced quadruped robots and some of them exhibit excellent performance, such as Stanford Doggo [2], Mini Cheetah [3], ANYmal [4], Stanford LittleDog [5], BigDog [6], HyQ [7], Tekken [8], MIT Cheetah [9].

Most of the quadruped robots mentioned above are designed with a rigid trunk, which only serves as a container for batteries, sensors, and auxiliary devices. Researchers have noted that trunk mobility can improve the locomotivity of legged animals and robots. The flexion and extension of the body contribute to the speed of mammals [10]. A jointed and segmented body provides functional flexibility and enhanced stability to arthropods [11, 12]. The effect of the spine on the maneuverability of quadruped robots has been investigated both in simu-

lation and experimentally in a wide range of topics and actions, such as bounding [13], stability [14], rapid acceleration [15], contact time [16], and energetic effect [17]. Nevertheless, these works studied the spine movement with a simplified model only considering the pitch motion of the trunk. Recently, the development of quadruped robots using metamorphic mechanisms [18] has attracted good interests. The continuous static gait [19], trot gait [20] and stability margin [21] of a quadruped robot with a twisting trunk were investigated, which demonstrated an improvement in locomotive performance with the metamorphic robot. Spyrakos-Papastavridis and Dai [22] proposed a model-free approach for stable-balancing and locomotion control of under-actuated, floating-base legged robots with contacts. This approach is based on the direct incorporation of power-shaping signal terms into the developed control laws [23, 24]. To the best of the authors' knowledge, there are very few quadruped robots that possess trunks with both pitching and twisting mobility [25]. As for their leg configuration, most quadruped robots have four similar mammal- or sprawling-type legs [26], and they are not able to change from one type to another. The sprawling-type configuration has advantages, such as improved stability, lower centre of gravity (COG), and wider range of motion. By contrast, the joint torques and footprints of mammal-like robots are relatively small. Note that, most quadruped robots are capable of only one type of mimicry, whilst those capable of multiple types of mimicry are rarely reported [27].

In previous works, Xu et al. [28] developed a reconfigurable quadruped robot whose every leg possesses 4 degrees of freedom (DOFs). This robot can change its leg configuration by locking different joints. Castano et al. [29] proposed CONRO robots - these are modular robots that can reconfigure their shapes by spliting into smaller robots or merging several modules to form a single larger hexapod robot. A reconfigurable hybrid hexapod robot that has 4 legs and 2 legs/arms was proposed in [30]. Two customized legs in its robot structure can be used as arms that can reach and hold objects. Jakimovski and Maehle [31] presented a self-reconfiguring hexapod robot dubbed OSCAR, which can amputate the malfunctioned legs, self-reconfigure and continue walking. Wheel-legged hexapod robots can perform the type of hybrid locomotion that combines legged motion and wheeled motion [32]. It is noticeable that most of the works above address quadruped/hexapod robots that achieve the reconfigurability by changing their legs. In addition, Gao et al. [33] designed an Origami-based hexapod robot (HexaMorph), which can perform simple tasks, such as self-deploying and locomotive squirming. Wu et al. [34] proposed an octopod platform with a reconfigurable trunk, which is a close-chain Bricard linkage with specific geometric constraints. This robot is able to adjust its trunk configuration so as to improve its locomotivity, while it cannot change between different types of mimicry. Different types of mimicry have advantages on different terrains. Developing a multi-mimicry reconfigurable quadruped robot with only one mechanical structure, also necessitates development of a sophisticated control system, which is a challenging task.

Metamorphic mechanisms [35, 36, 37, 38] featuring the ability to change their topology and mobility have been widely studied [39, 40, 41]. Each metamorphic linkage [42, 43, 44] has a configuration space that includes at least two subspace components that are connected by bifurcation singularities [45]. Therefore, the mechanism can work in different motion branches without reassembly. The change of link annexation or joint functionality leads to a change of motion branches, so as to achieve reconfiguration of the metamorphic mechanism [46]. For a metamorphic mechanism, the reconfiguration analysis aims to identify all the bifurcated branches and bifurcation singularities in its configuration space. The available approaches include the numerical method [47, 48], kinematic mapping method [49] and algebraic geometry approach [50]. Recently, a novel approach based on the higher-order kinematic analysis of spatial linkages was proposed [51, 52, 53, 54], which is efficient in the identification of motion branches at the bifurcation singularities of a metamorphic mechanism. Note that, the reconfigurability of a modular robot [55, 56], which is achieved by connecting and disconnecting modules [57, 58, 59], is different from that of a metamorphic mechanism.

The objective of this work is to develop a biomimetic quadruped robot capable of multiple types of mimicry. The main motivations for designing this robot are summarized as follows:

1. Taking advantage of its reconfigurability, a metamorphic mechanism is designed as the trunk of the quadruped robot so as to achieve reptile-, arthropod-, and mammal-like working modes within a single mechanical structure.
2. Unlike other related works, the relative positions and postures of the metamorphic robot's legs can be rearranged in a controllable way during its body reconfiguration so as to combine all the locomotion features of the three types of mimicry into one robot.
3. By virtue of the changeable and adaptable trunk, the metamorphic quadruped robot is capable of maintaining better adaptability and having more movement options in different environments, especially within extreme and restricted terrains, in comparison

Journal of Mechanisms and Robotics. Received December 01, 2021;
Accepted manuscript posted April 17, 2022. doi:10.1115/1.4054408

to the extant quadruped robots.

To achieve these goals, a metamorphic trunk based on an eight-bar, single-loop mechanism is designed and analyzed. Subsequently, four typical modes are selected for further development, and the transformation routes among all motion branches and bifurcation singularities are planned. The enhanced maneuverability of the proposed robot is investigated and demonstrated with some designed locomotion gaits and strategies, such as packaging itself automatically, self recovery, fast spinning (FSP) gait, stair climbing (STC) gait, as well as passing through right-angled bends and narrow spaces. Finally, both indoor and outdoor experiments are carried out to validate the superior adaptability and locomotivity of the multi-mimicry robot, as well as the effectiveness of the proposed gaits and strategies.

The rest of this paper is organized as follows: Section 2 outlines the main focuses in the design of the bio-inspired, multi-mimicry robot. The architectural design and configuration space of the metamorphic trunk are presented in Section 3. The four working modes along with the transformation routes of the proposed robot are introduced and illustrated in Section 4. In Section 5, the enhanced locomotivity of the multi-mimicry quadruped robot is analyzed and demonstrated. In Section 6, the enhancements provided by the multi-mimicry metamorphic robot and the proposed movement strategies are validated through both indoor and outdoor experiments. The conclusions of this work are presented in Section 7.

2 BIO-INSPIRED METAMORPHIC ROBOT DESIGN CONSIDERATIONS

To successfully endow legged robots with structures resembling those of their biological counterparts, it is important to understand their architectural properties. After investigating various animals, four points are to be considered in the biomimetic robot's mechanism design.

(a) (b) (c)

Fig. 1: Three typical legged animals: (a) leopard, (b) lizard, and (c) spider.

Legged animals are the most successful members of the terrestrial species largely because of the versatility of their limbs, in terms of adapting to complex terrains. The fish-tetrapod transition enabling the vertebrates to move on land is one of the greatest evolutionary events known [60]. Generally, the animals having weight-bearing and locomotive limbs can be divided into tetrapods [61, 62] (vertebrates with paired arms and legs) and arthropods [63, 64] (invertebrate animals possessing exoskeletons, segmented bodies, and paired jointed legs), which evolved legged locomotion capabilities independently.

The legs have provided the required agility to animals which have to adapt to complex environments. Quadruped mammals, including cattle, sheep, horses and leopards, tend to have strong and slender legs, which are located near the abdomen, as shown in Figure 1(a). When moving forward, the first joint of each leg (hip joint or shoulder joint) can be simplified as a revolute joint with an axis aligned horizontally. It is noted that many quadrupedal mammal gaits are the same as one another, due to the similar skeleton structures of these different animals, and this can be confirmed by determining the energetically-optimal gaits using a quadrupedal model [65]. Legged reptiles, such as geckos, lizards and tortoises, are quadrupedal animals having paired and relatively short and stubby legs, as shown in Figure 1(b). Unlike legged mammals, their legs are attached to the two opposite sides of the body, and the proximal joint of each of their legs is simplified as a revolute joint with a vertical axis, thus it is difficult for them to stand upright. Their movements constitute a classic crawl, using side-to-side gaits with substantial trunk bending. An arthropod body consists of segments joined together in a form similar to the revolute joint, and carries pairs of legs which are almost symmetrically distributed on either two opposite sides of the body or around the body. The movements of their segmented bodies enhance their stability during locomotion [12]. Some arthropods, such as spiders, mantises and locusts, possess relatively slender legs, and their second leg joints protrude upwards, as shown in Figure 1(c), which means that the reach range of each leg is relatively larger in comparison with its respective body size. Based on this observation, the mechanical differences among legged animals mostly lie in the size and configuration of the trunk, the structures and layouts of the joints, and the lengths and arrangements of the bones or exoskeletons.

For engineers, legged animals are the best imitation candidates for the design of artificial walking machines [66, 67, 68, 69]. Nevertheless, in comparison to robot walking, animal locomotion seems to be much more effective and versatile. Therefore, it is of significance to

consider the corresponding biological structures so as to apply similar mechanisms to legged robots. However, complete bionics are rarely successful due to the limits in control systems, actuators, sensors, materials, etc [12]. Since this work is concerned with the design of a quadruped robot capable of multiple types of mimicry, we will focus on only four aspects of mechanical features in animals, in an attempt to combine different biological architectures with various locomotive advantages. The four points considered in our design are listed as follows:

1. The twisting ability (bending horizontally) of the trunk.
2. The pitching ability (bending vertically) of the trunk.
3. The positional relationships between the trunk and the legs.
4. The positional relationships among different legs.

3 ARCHITECTURAL DESIGN AND CONFIGURATION SPACE OF THE METAMORPHIC TRUNK

Considering the four points listed in Section 2, a metamorphic trunk retaining the ability to change configuration is designed in this section.

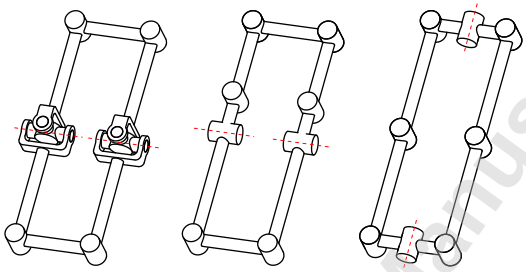

(a) (b) (c)

Fig. 2: Three typical trunks evolved from the planar six-bar mechanism by including two horizontally-arranged coaxial revolute joints: (a) configuration 1, (b) configuration 2, and (c) configuration 3.

3.1 Design of the Metamorphic trunk

We first designed a quadruped robot by employing a planar, six-bar mechanism trunk, which is able to twist and change the relative positions between the legs [20]. The planar six-bar mechanism has six revolute joints, the axes of which are parallel to each other. Subsequently, we tried to add another motion branch into the planar six-bar mechanism to endow the trunk with a pitching capability. The first solution that was attempted is the universal joint, namely a pair of symmetrically arranged revolute joints replaced by universal joints, as shown in Figure 2(a). If this mechanism is adopted as the trunk of the quadruped robot, at least one rotation axis of the universal joints should be active so as to enable pitching motion. However, it is difficult to install a motor near the universal joint due to the limitations of the installation space. Besides, the workspace of the universal joint is quite limited [70, 71, 72]. To overcome this problem, another two mechanisms were readily derived based on the approach presented in [39, 73, 74], as shown in Figures 2(b) and (c), which possess similar abilities to the one with universal joints.

The mechanism depicted in Figure 2(b) is derived based on the mechanism displayed in Figure 2(a) by separating the axes of each universal joint, thus it becomes an eight-bar mechanism. However, one of the twisting and pitching motions in this configuration cannot rotate around the geometric centerline of the trunk. As shown in Figure 2(c), the front and rear links of the trunk are bisected and joined/connected by two coaxial revolute joints. This bifurcation singular configuration has two motion branches, namely the planar six-bar mechanism branch and the kinematically-redundant Sarrus linkage branch [49].

In this work, the mechanism shown in Figure 2(c) was selected to serve as the metamorphic trunk of the bionic quadruped robot because of its symmetry. Thus the metamorphic trunk is composed of eight rigid links and eight revolute joints. As illustrated in Figure 3, the eight joints are denoted using A to H. The lengths of links BC, CD, FG and GH are equal to each other, and links AB, DE, EF and HA have the same lengths.

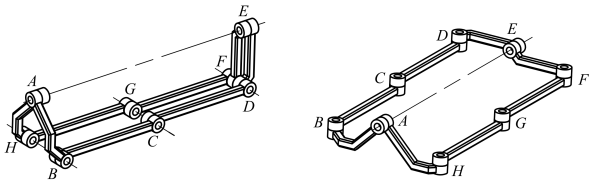

(a) (b)

Fig. 3: Sketches of the 8-bar metamorphic single-loop mechanism: (a) singular configuration 1, and (b) singular configuration 2.

Journal of Mechanisms and Robotics. Received December 01, 2021;
Accepted manuscript posted April 17, 2022. doi:10.1115/1.4054408

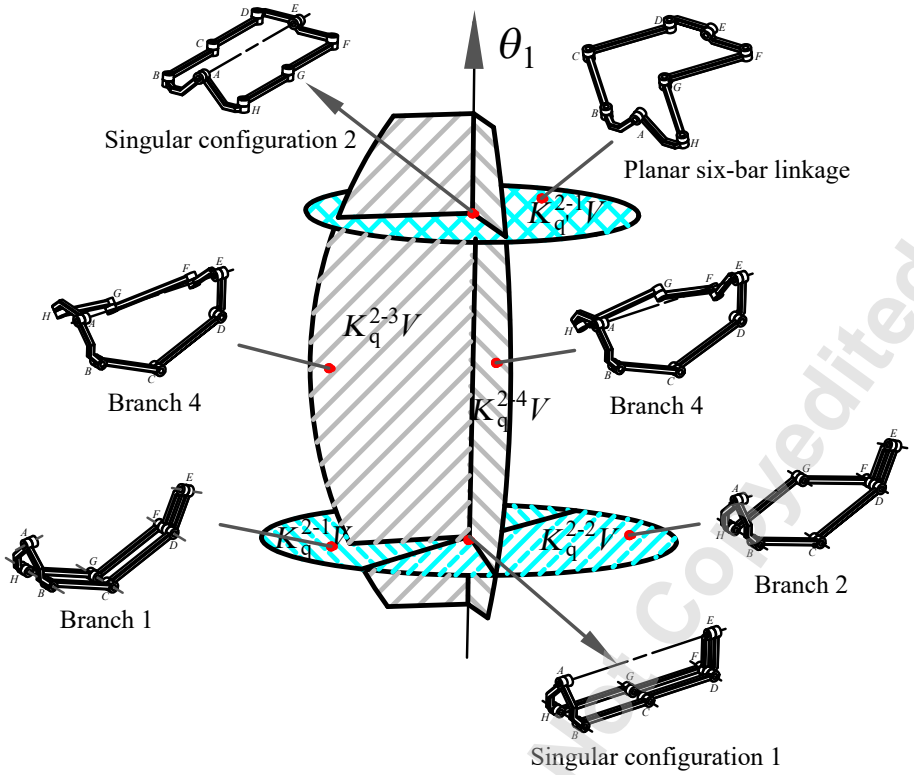

Fig. 4: Configuration space of the metamorphic trunk.

3.2 Configuration space of the metamorphic trunk

As analysed in our previous work [75], the metamorphic trunk has five motion branches, which are denoted by different surfaces in Figure 4. Singular configuration 1 is the intersection of branches $\boldsymbol{K}_{\boldsymbol{q}}^{2-1}\boldsymbol{V}$, $\boldsymbol{K}_{\boldsymbol{q}}^{2-2}\boldsymbol{V}$, $\boldsymbol{K}_{\boldsymbol{q}}^{2-3}\boldsymbol{V}$, and $\boldsymbol{K}_{\boldsymbol{q}}^{2-4}\boldsymbol{V}$. The branches $\boldsymbol{K}_{\boldsymbol{q}}^{2-3}\boldsymbol{V}$ ($\boldsymbol{K}_{\boldsymbol{q}'}^{2-2a}\boldsymbol{V}$), $\boldsymbol{K}_{\boldsymbol{q}}^{2-4}\boldsymbol{V}$ ($\boldsymbol{K}_{\boldsymbol{q}'}^{2-2b}\boldsymbol{V}$) and the planar six-bar linkage are connected by singular configuration 2. The planar six-bar linkage can be transformed to the branches $\boldsymbol{K}_{\boldsymbol{q}}^{2-1}\boldsymbol{V}$ and $\boldsymbol{K}_{\boldsymbol{q}}^{2-2}\boldsymbol{V}$ through branches $\boldsymbol{K}_{\boldsymbol{q}}^{2-3}\boldsymbol{V}$ and $\boldsymbol{K}_{\boldsymbol{q}}^{2-4}\boldsymbol{V}$, respectively. The adjacent branches are connected by a set of singularities, which is indicated by the intersection lines in Figure 4.

4 MULTI-MIMICRY QUADRUPED ROBOT

By employing the metamorphic eight-bar trunk, a novel biomimetic quadruped robot featuring multiple forms of mimicry is developed. In this section, the working modes of the robot are introduced, and the transformation routes among the modes are analyzed and planned.

4.1 Working modes

The biomimetic quadruped robot consists of a trunk and four identical legs, which are mounted onto the CD, FG, BC and GH links, respectively, as shown in Figure 5, where P_i represents the foothold of the ith leg. Each leg has three active revolute joints. In an analogous manner to animals existing in nature, the legs of the developed quadruped robot are symmetrically arranged. Owing to its reconfigurability, the robot can change its working modes according to the nature of the environment's terrain. In this work, four modes with various locomotion characteristics are selected for further development.

Mode 1: As depicted in Figure 5(a), the trunk of mode 1 is in the branch of $\boldsymbol{K}_{\boldsymbol{q}'}^{2-1}\boldsymbol{V}$, namely the planar six-bar mechanism, which can be reshaped on the plane that its links lie on. Similar to lizards, the robot is of bilateral symmetry, with an improved ability to move in the fore-aft direction, as compared to moving left and right. For this reason, in Section 5.2, a novel fast spinning gait (FSP) utilizing the twisting motion of the trunk is designed to improve the robot's turning ability.

Mode 2: As depicted in Figure 5(b), the trunk of mode 2 is also in the branch of the planar six-bar mechanism. Unlike mode 1, all interior angles of the trunk are

Journal of Mechanisms and Robotics. Received December 01, 2021;
Accepted manuscript posted April 17, 2022. doi:10.1115/1.4054408

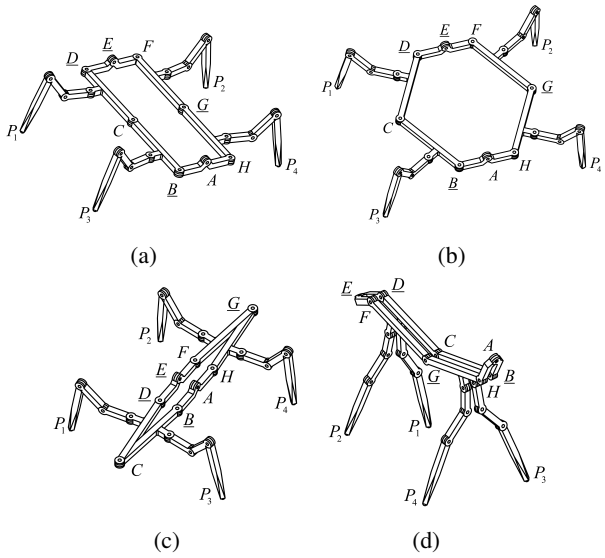

Fig. 5: The biomimetic quadruped robot: (a) mode 1, (b) mode 2, (c) mode 3, and (d) mode 4.

equal to 120°, and the legs are distributed centrosymmetrically around the trunk, thus it looks like a hexagon. In this mode, the robot imitates a four-legged spider which can walk equally well in both the fore-aft and lateral directions.

Mode 3: As shown in Figure 5(c), the reconfigurable trunk of mode 3 is in the branch of $\boldsymbol{K}_{\boldsymbol{q}}^{2-3}\boldsymbol{V}$. The trunk of this mode has two motions, namely a rotation around the collinear axes of joints A and E, and a translation of an equivalent Sarrus linkage when the revolute joints A and E are fixed. In this mode, the robot is similar to an arthropod with a body consisting of two sections being able to rotate around each other (pitch upwards or downwards). Owing to the pitching ability offered by the rotation, the robot is skilled at climbing vertical obstacles. Besides, the width of the quadruped robot is changeable during translational mobility. Thus mode 3 also renders the robot adroit at crawling through narrow paths. In Section 5.3, a novel stair climbing gait (STC) empolying the pitching motion of the trunk is designed and analysed to demonstrate the robot's locomotion advantages.

Mode 4: As shown in Figure 5(d), the robot is shaped like a legged mammal, the legs of which are underneath the trunk. The metamorphic trunk becomes a 3-DOF serial mechanism, which can be divided into four segments, including the head, front trunk, rear trunk and tail. The head and tail help increase the locomotive velocity and equilibrate the feet–ground reaction forces [76]. Furthermore, the pitching motion between the front trunk and the rear trunk enables the robot to regulate the location of the centre of gravity, which ensures that the robot is skilled at crawling over a variety of surfaces in unstructured environments. Besides, the footprint of mode 4 is much smaller than the other three modes, thus it is better at passing through narrow passages.

After determining the working modes of the metamorphic trunk, the combination of active joints can be determined, which is defined as the union of actuated joints required for the control of each branch that the robot passes through. As each motion branch may have multiple combinations of actuated joints, the optimal actuation scheme should have the least number of actuated joints. In addition, factors such as interferences, workspace and singularities also need to be considered during the design of the actuation scheme. For the metamorphic quadruped robot, joints B, D, E and G, which are indicated by underlined letters in Figure 5, are selected to fully control the metamorphic trunk. However, in some singular configurations (eg. singular configuration 1), the trunk is underactuated and seems to be intractable. To avoid this, some strategies are applied, such as those introduced in Section 4.2.

In order to be able to coexist with other control algorithms, a joint-level control method with predefined trajectories is adopted in this work to avoid issues such as interferences, joint limits, or singularities. Each working mode employs an inverse kinematics solver associated with its configuration and structural parameters. The switching between different working modes can be achieved with a state machine, in which each state corresponds to several terrains for which the robot possesses heightened locomotion capabilities. The surrounding environment of the robot can be detected with complex sensing devices and algorithms [77]. When entering a new terrain, the robot switches from an inverse kinematics solver to a predefined trajectory to perform the mode-switching action. The locomotive performances of modes 1-4 in various terrains are qualitatively presented in Table 1, where the greater the number of stars, the better the locomotive ability.

4.2 Transformation route planning

Based on the configuration space established in Section 3.2, the transformation routes of the biomimetic quadruped robot can be mapped, as shown in Figure 6. In both modes 3 and 4, the metamorphic quadruped robot is able to package itself for easy transportation by automatically folding itself into a cuboid configuration. Therefore, it can be potentially used in scenarios such as field mapping and planetary exploration [78, 79], where the volume of transportation equipment is an expensive premium.

Journal of Mechanisms and Robotics. Received December 01, 2021;
Accepted manuscript posted April 17, 2022. doi:10.1115/1.4054408

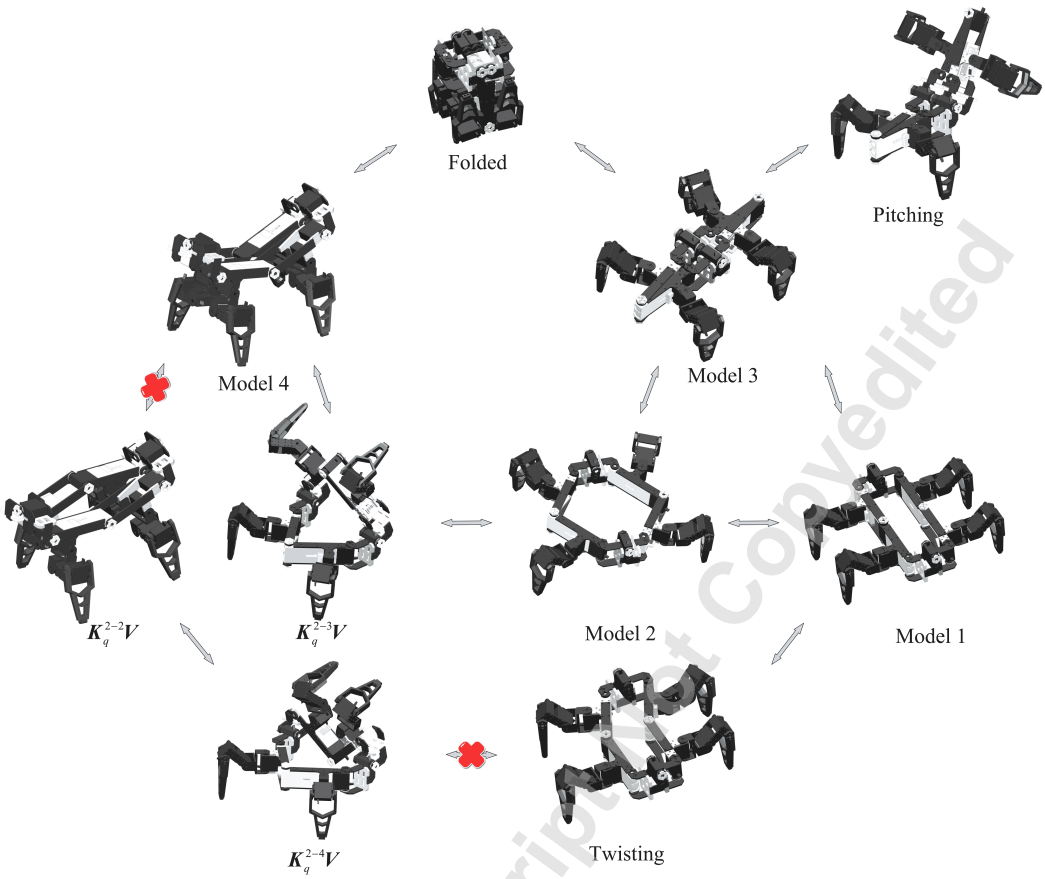

Fig. 6: Transformation routes of the biomimetic quadruped robot.

Table 1: Performances of six typical locomotions of modes 1-4.

	Fore-aft crawl	Lateral crawl	Spinning	Overcoming obstacles	Narrow path	Uneven surface
Mode 1	⋆⋆⋆⋆⋆	⋆⋆⋆	⋆⋆⋆⋆⋆	⋆⋆⋆	⋆⋆⋆	⋆⋆⋆
Mode 2	⋆⋆⋆	⋆⋆⋆⋆⋆	⋆⋆⋆⋆	⋆⋆⋆	⋆⋆	⋆⋆⋆
Mode 3	⋆⋆⋆⋆	⋆⋆⋆	⋆⋆⋆⋆	⋆⋆⋆⋆⋆	⋆⋆⋆⋆	⋆⋆⋆⋆⋆
Mode 4	⋆⋆⋆⋆	⋆⋆	⋆⋆⋆	⋆⋆⋆⋆	⋆⋆⋆⋆⋆	⋆⋆⋆⋆

It is demonstrated in Figure 6 that modes 1, 2 and 3 can be readily converted to into one another, while mode 4 is relatively independent, and cannot be directly transformed into the other three modes, and vice versa. There are two possible routes from the planar six-bar linkage branch to mode 4, through the branch $\boldsymbol{K_q^{2-3}V}$ or branches $\boldsymbol{K_q^{2-4}V} - \boldsymbol{K_q^{2-2}V}$. Nevertheless, in both branches $\boldsymbol{K_q^{2-2}V}$ and $\boldsymbol{K_q^{2-4}V}$, the joints C and G of the trunk protrude in nearly opposite directions, which gives rise to a peculiar looking configuration and increases the possibility of interference between one pair of legs. Accordingly, the "safer" transformation route from mode 1 to mode 4 is the one passing through mode 2 and branch $\boldsymbol{K_q^{2-3}V}$. The whole transformation process can be divided into four steps: (a) The robot extends the width of its trunk by simultaneously reducing the interior angles $\angle BCD$ and $\angle HGF$. (b) The robot rotates one half of the trunk along the collinear axes of joints A and E, and the

Journal of Mechanisms and Robotics. Received December 01, 2021;
Accepted manuscript posted April 17, 2022. doi:10.1115/1.4054408

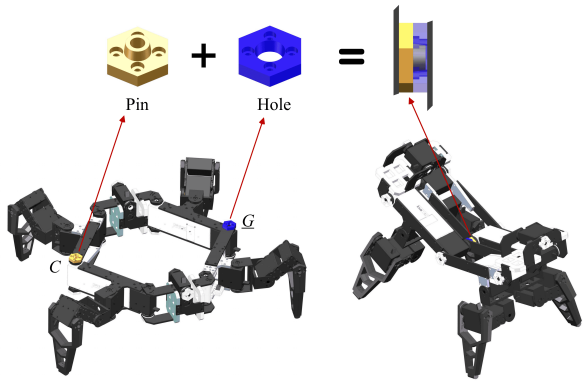

Fig. 7: Pin-hole component to avoid unwanted transformations

footholds P_1 (P_2) and P_3 (P_4) are moved to maintain balance. (c) The robot increases the interior angles $\angle BCD$ and $\angle HGF$, and stands up with the help of four legs. (d) The robot rotates its head and tail, thus the axes of joints A and E are no longer collinear, and the robot completely switches to mode 4.

In mode 4, the metamorphic trunk is singular when the joints B, C, D, F, G and H are coplanar, and may fall into the branch $\boldsymbol{K}_{\boldsymbol{q}}^{2-2}\boldsymbol{V}$. In order to avoid such a situation, a pin-hole gadget is designed to ensure that the axes of joints C and G are collinear and rotate at the same speed. As shown in Figure 7, the "Pin" part has the same axis as joint C and is fixed above joint C. Similarly, the "Hole" part is attached to joint G and has the same axis as joint G. When reshaping into mode 4, the "Pin" sticks into the "Hole" to form a hinge connection.

5 ENHANCED LOCOMOTIVITY

In most quadruped robot designs, the trunks are designed as rigid bodies and cannot be adapted to improve their locomotivity. With the inclusion of a metamorphic trunk, the biomimetic quadruped robot acquires a configuration adjustment ability, which leads to improved adaptability to various environments. In this section, examples are included to demonstrate the enhanced locomotive performance of the proposed robot.

5.1 Fall recovery

When looking at state-of-the-art fall recovery of quadruped robots, we find that most of them are not able to recover from a falling pose, limiting their applicability to real-world tasks. Thus it is necessary to design a precise sequence of motions that allows the robot to execute a desired gait after a fall.

By observing animals in nature, we found that there are three key points pertaining to self recovery:

1. The shape and mobility of the trunk. We compare two reptiles: the tortoise and crocodile. The trunk of the tortoise is quasi-circular, which means that the dimensions in all directions are similar. By contrast, the trunk of the crocodile is slender and its length is much longer than its width. For a tortoise, it is hard to turn over when sprawling on the ground, while there are numerous recorded instances of crocodiles spinning along the axis parallel to their spines. In addition, the mobility of the trunk also has a great impact on their fall recovery ability. This is because the flexible trunk can change the relative position of each leg and more importantly enlarge its workspace. For a more detailed workspace analysis, please refer to a screw-based approach presented in [80].
2. The mobility of the leg, which includes two aspects, namely the position and structure of each leg, as well as its workspace. The preferred locomotive direction of a legged animal depends largely on the positions and mechanical structures of its legs. In their preferable directions of movement, they tend to exhibit improved stability and maneuverability, although it becomes more difficult to roll over. It is known that crabs walk sideways on land, and the mobility of their legs is relatively limited in the fore-and-aft direction. The best direction for a crab to turn over is the fore-and-aft one. The spider has a quasi-circular body, and its legs are relatively slender and circularly distributed, which provides it with a large leg workspace and abundant direction-of-motion choices. Thus it can roll over easily in all directions.
3. The auxiliary physical support of the body, such as the head of a camel, the trunk of an elephant and the tail of a scorpion, which are typically used in the fall recovery process. These parts can serve as fulcrums away from the body and provide external forces when rolling over.

In terms of legged robots, bipedal humanoids possessing relatively slender limbs with large workspaces are able to stand up by supporting themselves with their legs and arms, and by following a sequence of contact states [81]. Utilizing six legs to increase the number of support points, a solution was proposed by Peng [82] to enable hexapod robots to perform self-recovery movements. Nevertheless, it is more challenging to implement the methods above for a quadruped robot, as the structural constraint of the quadruped robot having only four

Journal of Mechanisms and Robotics. Received December 01, 2021;
Accepted manuscript posted April 17, 2022. doi:10.1115/1.4054408

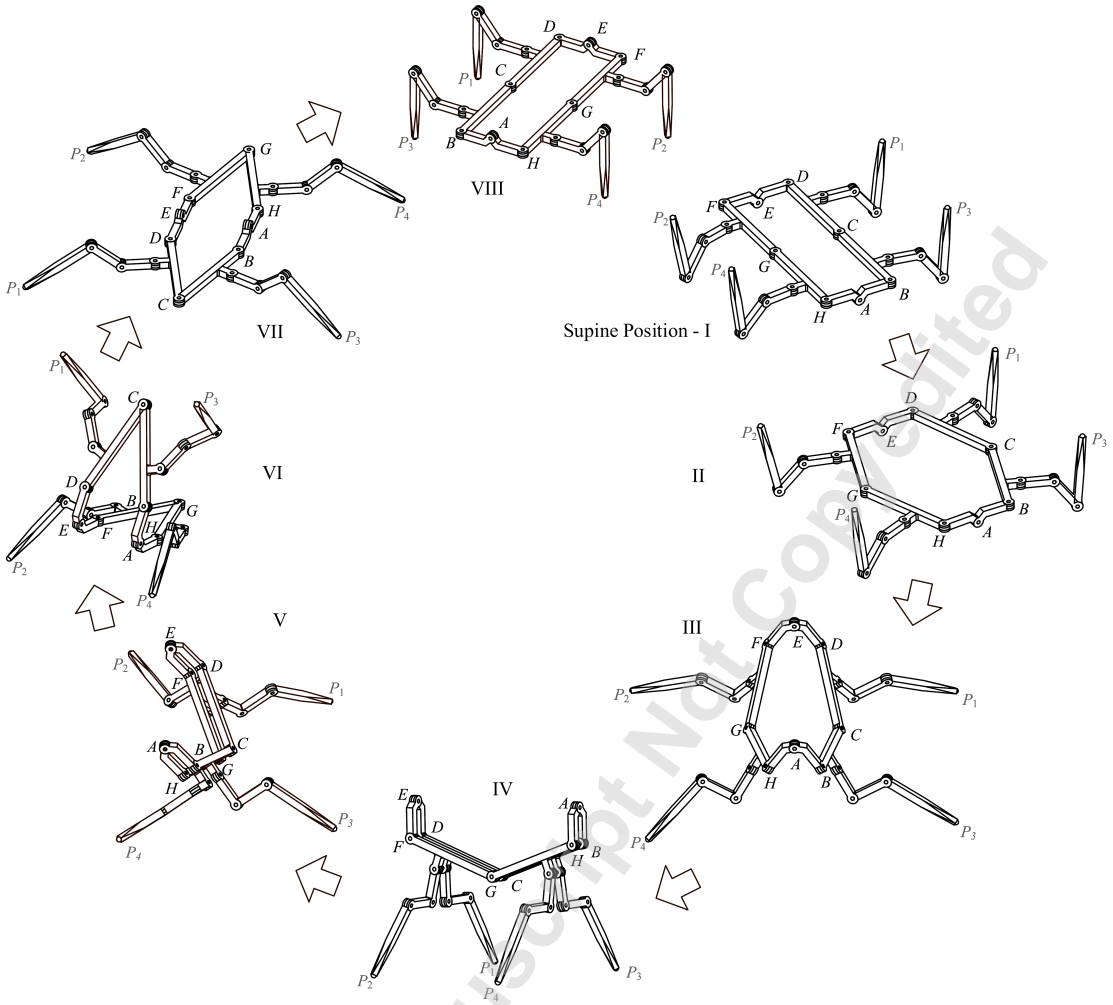

Fig. 8: Reconfiguration motion of the biomimetic quadruped robot during the fall recovery process.

legs leads to a lack of support points. Besides, as a consequence of pursuing good mobility and agility, the restrictions of power, weight and space do not allow the quadruped to be equipped with long extensible arms and other auxiliary devices. Some quadruped robots, such as the HyQ [83] and ANYmal [4], can lie on one side after a fall due to the special designs of their COG locations and trunk shapes. Thus it is easy for them to recover after falling on the ground. The latest SpotMini of Boston Dynamics has a 6-DOF arm on its trunk, which can provide a support force when getting up [84]. With consideration of passive elastic elements, Spyrakos-Papastavridis et al. [85, 86, 87, 88] presented an in-depth study on the stability and balance control of legged systems. Recently, a multiexpert learning architecture that can learn to generate fall recovery actions was proposed [89]. In this section, an alternative static strategy was proposed to endow quadruped robots, especially those in supine positions, with self-recovery capabilities. By taking advantage of the metamorphic trunk, the fall recovery process depicted in Figure 8 is implemented in six steps.

Step 1: The robot changes its trunk into a hexagonal shape from a rectangular shape. As in the rectangle configuration, the metamorphic trunk is singular, which means its configuration may be transferred into an unexpected motion branch. To be exact, if Leg 1 and Leg 3 support the robot's body on the ground, a force will be applied to links FG and GH, which will make the trunk change into the branch $\boldsymbol{K}_{\boldsymbol{q}}^{2-4}\boldsymbol{V}$, as shown in Figure 9. The purpose of Step 1 is to avoid this situation.

Step 2: The robot reshapes its trunk by rotating along the collinear axes of A and E. The footholds of all four

Journal of Mechanisms and Robotics. Received December 01, 2021;
Accepted manuscript posted April 17, 2022. doi:10.1115/1.4054408

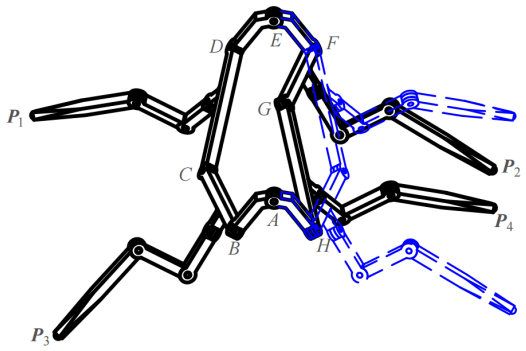

Fig. 9: Sketch of the two possible transformations associated with $\boldsymbol{K}_{\boldsymbol{q}}^{2-4}\boldsymbol{V}$ and $\boldsymbol{K}_{\boldsymbol{q}}^{2-3}\boldsymbol{V}$ (dotted lines).

legs are located on the ground. The robot transforms into the motion branch $\boldsymbol{K}_{\boldsymbol{q}}^{2-3}\boldsymbol{V}$, as shown in Figure 8-III. After this step, the robot reshapes its trunk into mode 4.

Step 3: The robot futher adjusts its trunk and moves its legs to stand on the ground in mode 4, as shown in Figure 8-IV.

Step 4: Mode 4 of the robot uplifts legs 2 and 4, allowing the robot to lie down, as shown in Figure 8-V. Meanwhile, these two legs rotate their joints, and their shins support the robot's body on the ground. Besides, the robot curls up its body and moves its head close to its tail. The robot will transfer itself into a pose in which its two left toes (P_2 and P_4) are far away from the body.

Step 5: The robot lifts half of its body (linkage $ABCDE$) by rotating along AE. As there is a stable support triangle $\triangle P_2P_4G$, the robot remains in a multi-contact state, as shown in Figure 8-VI. After a rotation of 180 degrees, the trunk is transformed into a shuttle-like configuration, as shown in Figure 8-VII.

Step 6: The robot stands up, and its trunk is restored to its rectangular shape.

Compared to bipedal configurations, the quadrupedal configuration provides an enhanced intrinsic balancing ability because of its larger support polygon, albeit at the expense of making it more difficult for the quadruped to recover from a supine pose. By transforming into mode 4, the robot becomes much more slender, which significantly reduces the energy required to roll over. Besides, in the configuration of mode 4, all the legs of this robot are mounted below its trunk, which also considerably diminishes the energy stability margin [90]. The best direction for executing the mode 4 recovery procedures is the right-left one, in which each leg has the largest motion range [25]. As a result, the robot can easily move towards the side-lying position by lifting legs 2 and 4 and extending legs 1 and 3, as shown in Figure 8-V.

5.2 Fast spinning

In this section, we look into the gait design corresponding to the twisting capability. In mode 1, the trunk of the six-bar mechanism endows the body with 3 DOFs, namely two translations in the link plane and one rotation about an axis perpendicular to the link plane. The effect of the twisting trunk on the gaits responsible for movement in the fore-and-aft direction has been investigated [20, 19, 21]. In this section, a novel FSP gait is proposed to demonstrate how the twisting trunk contributes to the turning motion.

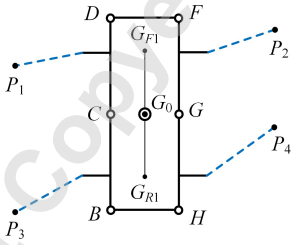

Fig. 10: A simplified model of the metamorphic quadruped robot in mode 1.

5.2.1 *Design of the FSP gait with mode 1*

For simplification, the revolute joints A and E are disregarded, thus BH serves as one link as well as DF. The whole trunk is divided into two halves by the line CG: the front one (Linkage $CDFG$) and the rear one (Linkage $BCGH$), as shown in Figure 10, where G_0 represents the COG of the biomimetic quadruped robot (the mass centre of the robot with four massless legs), G_{F1} and G_{R1} denote the COGs of the front and rear halves, respectively. By virtue of the symmetry of the trunk, G_0 is located at the midpoint of G_{F1} and G_{R1}.

The spinning gait of a quadruped robot with a rigid trunk can be divided into six steps, with four steps for leg transferring and two steps for trunk rotating [91]. This gait is discontinuous, because the foot-placing and trunk-turning sequences are implemented sequentially. By utilizing the twisting motion, these two types of movements can be implemented simultaneously, thus reducing the number of gait steps and increasing the spinning speed.

For the proposed FSP gait, the spinning centre is a fixed point located at the midpoint of CG. It is noted that the spinning direction can be either anticlockwise or clockwise. In this section, we take the clockwise spinning as an example to present the FSP gait. The robot rotates

Journal of Mechanisms and Robotics. Received December 01, 2021;
Accepted manuscript posted April 17, 2022. doi:10.1115/1.4054408

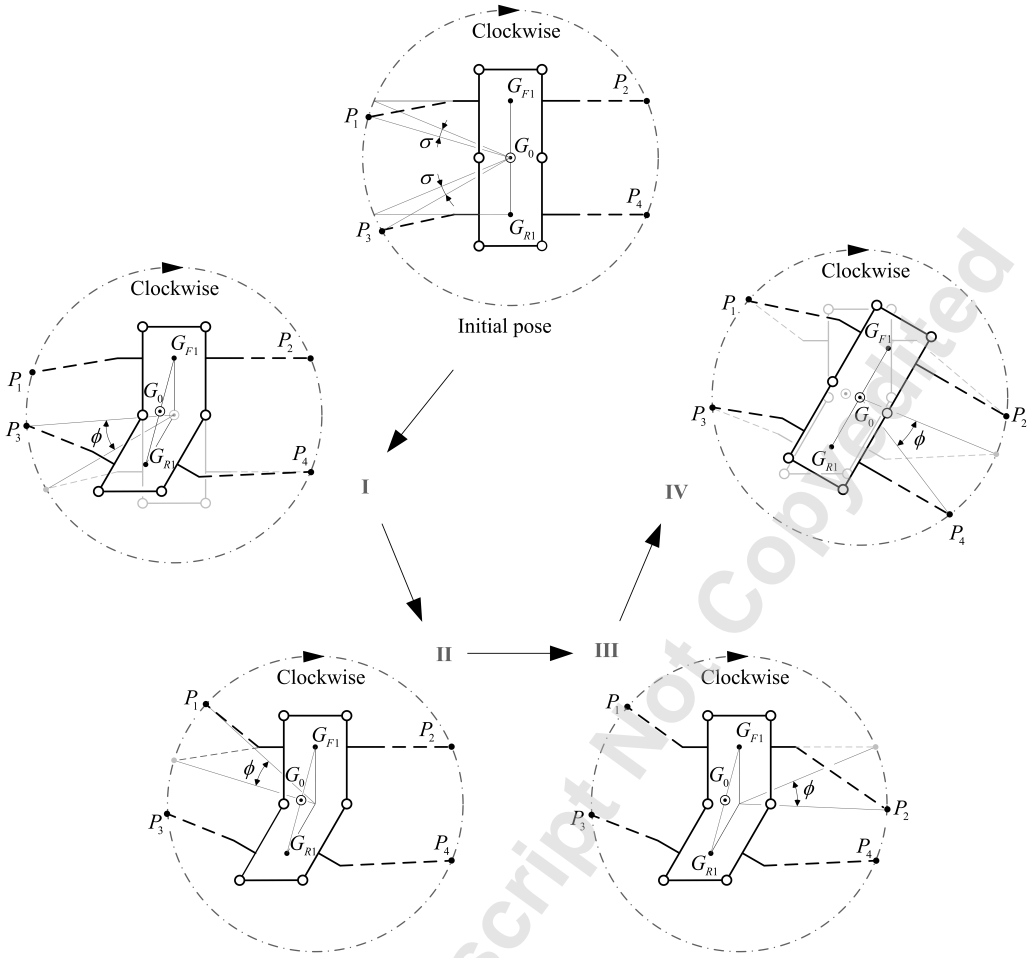

Fig. 11: The motion sequences of the periodic clockwise FSP gait in one period.

around the spinning centre about an angle of ϕ. Each foothold P_i traces a circle centred at the spinning centre, thus the displacement of each foothold can be represented by a central angle. At the start of each gait period, the trunk is shaped like a rectangle, and the footholds P_2 and P_4 are located at their initial positions (the middle of the leg workspace), whilst the footholds P_1 and P_3 have rotated anticlockwise about σ from their initial positions so as to keep the robot stable when turning, as depicted in Figure 11. The FSP gait will be implemented in four steps:

Step I: The rear half of the trunk twists clockwise by an angle ϕ, and leg 3 moves clockwise around the spinning centre about an angle ϕ. The front half of the trunk remains unchanged, keeping legs 1 and 2 in situ. In conjunction with the trunk motion, the configuration of leg 4 changes.

Step II: The trunk remains unchanged, keeping legs 2, 3 and 4 in situ. Leg 1 moves clockwise around the spinning centre by an angle ϕ.

Step III: The trunk remains unchanged, keeping legs 1, 3 and 4 in situ. Leg 2 moves clockwise around the spinning centre by an angle ϕ.

Step IV: The front half of the trunk twists clockwise by an angle ϕ, and leg 4 moves clockwise around the spinning centre by an angle ϕ. In conjunction with the trunk motion, the configurations of legs 1, 2 and 3 change.

It is noted that Steps 2 and 3 are similar to those of the gait presented in [91]. Due to the reduced number of steps, the FSP gait is expected to take less time than the conventional spinning gait designed for quadruped robots with rigid trunks.

Journal of Mechanisms and Robotics. Received December 01, 2021;
Accepted manuscript posted April 17, 2022. doi:10.1115/1.4054408

5.2.2 *Stability margin analysis of the FSP gait*

The COG changes with the twisting motion of the reconfigurable trunk, thus affecting the performance of the biomimetic quadruped robot. For four-legged robots, the stability margin is one of the most important performance criteria, as it reveals how stable the walking robot is. Among various stability margins, the static stability margin (SSM) is selected for the stability analysis, which is defined as the smallest distance from the projection of the COG on the ground to the edges of the convex support polygon formed by the footholds [92].

In this section, Step 1 is selected to demonstrate the calculation of the gait stability margin. As displayed in Figure 12, in order to simplify the calculation, the coordinate system $o-xy$ is fixed on the front half of the trunk, with its origin located at the midpoint of CG; x-axis pointing from C to G, and y-axis parallel to the vector pointing from C to D. When the rear half of the trunk rotates around o by an angle φ, the position vector of G_{R1} is given as

$$\boldsymbol{P}_{G_{R1}} = -d \begin{bmatrix} \sin(\varphi) \\ \cos(\varphi) \end{bmatrix} \tag{1}$$

where d denotes the distance between o and G_{R1}. The position vector of G_{F1} is

$$\boldsymbol{P}_{G_{F1}} = \begin{bmatrix} 0 \\ d \end{bmatrix} \tag{2}$$

Thus the position vector of G_0 is obtained by

$$\boldsymbol{P}_{G_0} = \frac{d}{2} \begin{bmatrix} -\sin(\varphi) \\ 1-\cos(\varphi) \end{bmatrix} \tag{3}$$

In Step I of the FSP gait, the support polygon is a triangle $\triangle P_1P_2P_4$, as in Figure 12, where $|P_2P_4| = 2d_2$, and R is the radius of the circumscribed circle of $\triangle P_1P_2P_4$. The position vectors of the three vertices of $\triangle P_1P_2P_4$ can be expressed as

$$\begin{aligned} \boldsymbol{P}_1 &= R \begin{bmatrix} -\sin\left(\operatorname{atan}\left(\frac{\sqrt{R^2-d_2^2}}{d_2}\right)+\sigma\right) \\ \cos\left(\operatorname{atan}\left(\frac{\sqrt{R^2-d_2^2}}{d_2}\right)+\sigma\right) \end{bmatrix} \\ \boldsymbol{P}_2 &= \begin{bmatrix} \sqrt{R^2-d_2^2} \\ d_2 \end{bmatrix}, \boldsymbol{P}_4 = \begin{bmatrix} \sqrt{R^2-d_2^2} \\ -d_2 \end{bmatrix} \end{aligned} \tag{4}$$

From Eqs. 3 and 4, the distance d_{ij} from G_0 to the edge P_iP_j of $\triangle P_1P_2P_4$ are solved by

$$d_{12} = \frac{|(x_1-x_G)(y_2-y_G)-(x_2-x_G)(y_1-y_G)|}{\sqrt{(x_1-x_2)^2+(y_1-y_2)^2}} \tag{5a}$$

$$d_{14} = \frac{|(x_1-x_G)(y_4-y_G)-(x_4-x_G)(y_1-y_G)|}{\sqrt{(x_1-x_4)^2+(y_1-y_4)^2}} \tag{5b}$$

$$d_{24} = \sqrt{R^2-d_2^2}+\frac{d}{2}\sin\varphi \tag{5c}$$

where $(x_i,\ y_i)$ represents the coordinates of P_i with respect to $o-xy$, and $(x_G,\ y_G)$ denotes the coordinates of G_0. The static stability margin (SSM), based on its definition, can be obtained by

$$\text{SSM} = \min(d_{12},\ d_{14},\ d_{24}) \tag{6}$$

After calculating the stability margin of the other three steps, the variation curve of the stability margin during one gait period can be obtained, as seen in Figure 13. The geometrical parameters are given as R=230mm, d_2=90mm, d=95mm, ϕ=45°, and σ=22.5°. It is found that the minimum stability margin value arises in Step II, and is equal to 9mm, while Step III has the maximum stability margin, which is equal to 47mm. In Step II and Step III, the SSM is constant, as one leg is lifted and the trunk does not change its configuration. The twisting motion of the trunk has an effect on the COG location, thus the SSM in Step I and Step IV is constantly changing. At the switching point of each step, the SSM value varies, because the leg-lifting movement leads to a change of the support triangle.

5.3 Stair climbing

In this section, we look into the design of the STC gait considering the pitching capability, along with an analysis that reveals the corresponding performance improvements.

5.3.1 *Design of the STC gait with mode 3*

For the sake of simplification, the translational mobility of the trunk in mode 3 is not taken into consideration. The body of the biomimetic robot can be simplified as two halves by a virtual revolute joint J_{AE} (Coaxial joints A and E): the front one (Linkage $EFGHA$)

Journal of Mechanisms and Robotics. Received December 01, 2021;
Accepted manuscript posted April 17, 2022. doi:10.1115/1.4054408

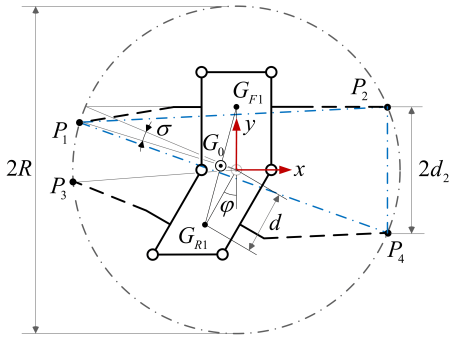

Fig. 12: A schematic diagram of the biomimetic quadruped robot in Step I of the FSP gait.

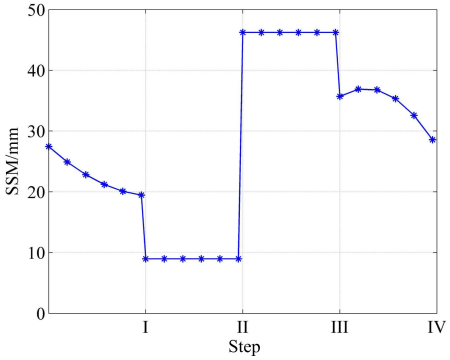

Fig. 13: The stability margin curve of the FSP gait during one period ($\phi = 45°$).

and the rear one (Linkage $ABCDE$), as shown in Figure 14, where α stands for the angle made by the front and rear halves of the trunk, and G_0 denotes the COG of the robot, G_{F2} and G_{R2} represent the COG of the front and rear halves of mode 3. Due to the structural symmetry of the trunk, G_0 is located at the midpoint of G_{F2} and G_{R2}. Note that, the front and rear segments of mode 3 are the right and left halves of mode 1, respectively. The coordinate system $o - xyz$ is fixed at the midpoint of A and E, with its y axis pointing from A to E, z axis pointing along the direction opposite to gravity, with the x axis being determined by the right-hand rule.

At the beginning of a gait cycle of the STC gait, both the front and rear halves of the trunk are parallel to the level ground ($\alpha = 0$), and legs 3 and 4 are in the middle of their reachable workspaces, while legs 1 and 2 have rotated anticlockwise around the z axis by σ. The STC gait will be implemented via the following procedures:

Step 1: Leg 1 moves forward by a length of s_{leg} (the projection of the displacement on the x axis). The configurations of the trunk and the remaining legs remain unchanged.

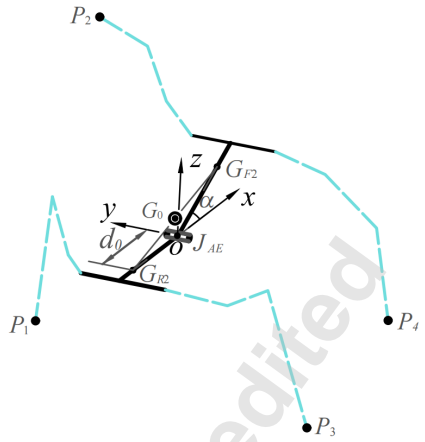

Fig. 14: The simplified model of the biomimetic quadruped robot in mode 3.

Step 2: The front half of the trunk rotates clockwise about the y axis ($\alpha > 0$). The configuration of leg 4 changes in conjunction with the rotation of the trunk.

Step 3: Leg 2 moves forward by a length of s_{leg}, and its foothold is placed on the stair.

Step 4: The geometrical center o of the trunk moves forward by a length of s_{trunk} (the projection of the displacement on the x axis). The configurations of the four legs change in conjunction with the trunk motion, while keeping their footholds in situ.

Step 5: Leg 3 moves forward by a length of s_{leg}. The configurations of the trunk and the remaining legs remain unchanged.

Step 6: Leg 4 moves forward by a length of s_{leg}, and is placed on top of the stair. The configurations of the trunk and the remaining legs remain unchanged.

Step 7: The geometrical center o of the trunk moves forward by a length of s_{trunk}. The configurations of the four legs change in conjunction with the trunk motion, while keeping their footholds in situ.

Step 8: The front half of the trunk rotates anticlockwise about the y axis ($\alpha < 0$). The configurations of the four legs change in conjunction with the trunk rotation, while keeping their footholds in situ.

Step 9: Leg 1 moves forward by a length of s_{leg}. The configurations of the trunk and the remaining legs remain unchanged.

Step 10: Leg 2 moves forward by a length of s_{leg}. The configurations of the trunk and the remaining legs remain unchanged. Up to now, half of the gait cycle is accomplished, the footholds of legs 2 and 4 are placed on

the stair, while legs 1 and 3 are still supporting the robot above the ground.

Step 11: The geometrical center o of the trunk moves forward by a length of s_{trunk}. The configurations of the four legs change in conjunction with the trunk motion, while keeping their footholds in situ.

Step 12: Leg 3 moves forward by a length of s_{leg} and will be placed on the stair. Legs 1, 2 and 4 remain in situ.

Step 13: Leg 4 moves forward by a length of s_{leg}. Legs 1, 2 and 3 remain in situ.

Step 14: This step is similar to Step 11. The geometrical center o of the trunk moves forward by a length of s_{trunk}. The four legs move in conjunction with the trunk motion, while their footholds remain unchanged.

Step 15: Leg 1 is placed on the stair by moving forward by a length of s_{leg}. Legs 2, 3 and 4 remain in situ.

Step 16: Leg 2 moves forward by a length of s_{leg}. The configurations of the trunk and the remaining legs remain unchanged.

Step 17: The rear half of the trunk rotates anticlockwise about the y axis until $\alpha = 0$. The trunk moves forward by a length of s_{trunk}. The configurations of the four legs change in conjunction with the trunk motion, while keeping their footholds in situ. After this step, the robot is already standing on the stair.

Step 18: Leg 3 moves forward by a length of s_{leg}. Legs 2, 3 and 4 remain in situ.

Step 19: Leg 4 moves forward by a length of s_{leg}. The configurations of the trunk and the remaining legs remain unchanged.

Step 20: The trunk moves forward by a length of s_{trunk}, and the robot recovers its initial configuration. The configurations of the four legs change in conjunction with the trunk motion, while keeping their footholds in situ.

During a single gait cycle, the trunk moves forward by a length of S_{stc}, which is larger than or equal to the length of the trunk. Each of the legs moves forward by a length of $3s_{leg}$, and the geometrical center of the trunk moves forward by $6s_{trunk}$. In order to recover the initial configuration, the following must be satisfied

$$S_{stc} = 3s_{leg} = 6s_{trunk} \tag{7}$$

5.3.2 *Stability margin analysis of the STC gait*

In this section, we take Step 3 and Step 12 as examples to calculate the stability margin of the biomimetic quadruped robot. We first look into the postural stability of Step 3, in which the reachable workspaces of legs 2 and 4 are lifted up with the pitching motion of the trunk. If the rear half of the trunk is parallel to the horizontal plane, and the front half of the trunk has rotated clockwise around the y axis by a value of α, the position vector of G_{F2} can be expressed as

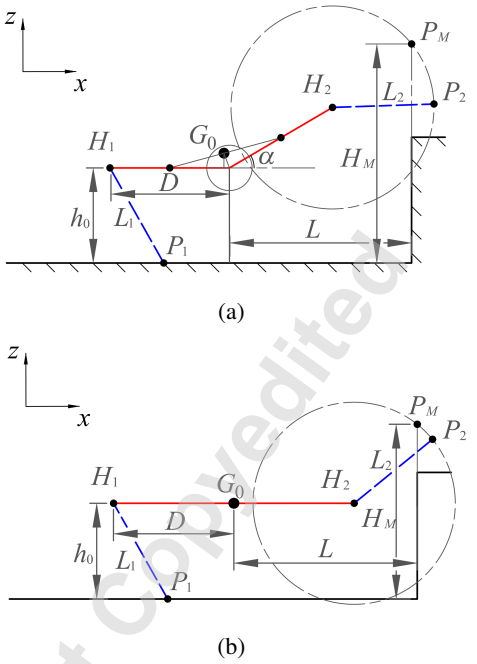

Fig. 15: The simplified models of the robot (Step 3) projected on the xz plane: (a) with a pitching trunk, and (b) with a rigid trunk.

$$\boldsymbol{P}_{G_{F2}} = [d_0\cos\alpha,\ 0,\ d_0\sin\alpha]^T \tag{8}$$

where d_0 denotes the distance between G_{F2} and o, which is equal to the distance between G_{R2} and o. The position vector of G_{R2} is given as

$$\boldsymbol{P}_{G_{R2}} = [-d_0,\ 0,\ 0]^T \tag{9}$$

Accordingly, the position vector of G is obtained by

$$\boldsymbol{P}_{G_0} = [-d_0\,(1-\cos\alpha)\,/2,\ 0,\ d_0\cos\alpha/2]^T \tag{10}$$

The projection of a simplified robot (Step 3) onto the xz plane is displayed in Figure 15(a), where H_i represents the hip joint of leg i, L_i denotes the distance between the hip joint and the foothold of leg i, D represents

Journal of Mechanisms and Robotics. Received December 01, 2021;
Accepted manuscript posted April 17, 2022. doi:10.1115/1.4054408

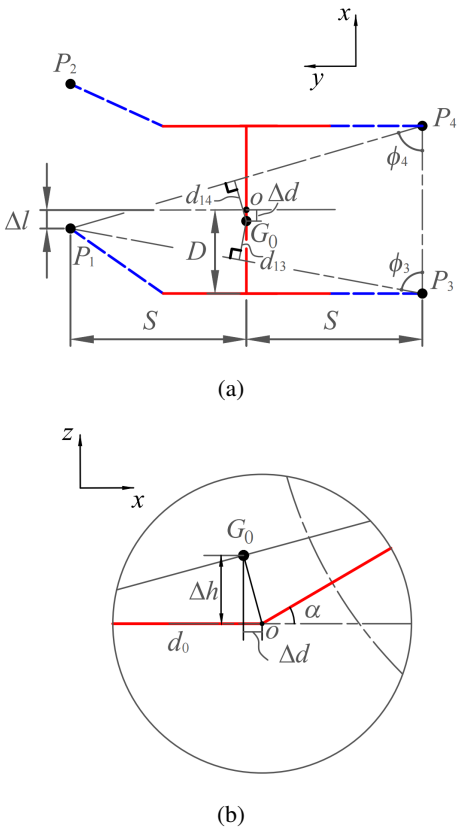

Fig. 16: The COG position of the biomimetic quadruped robot in Step 3: (a) projected on xy plane, and (b) projected on xz plane.

the distance between the joint H_i and the geometrical center of the trunk o, L denotes the distance between o and the vertical plane of the stair, and h_0 represents the distance between o and the level ground. For a comparative analysis, a similar robot without pitching mobility is also depicted in Figure 15(b). Here P_M represents the highest point of the stair that the robot can reach, which is defined as the highest intersection point between the line projected by the vertical plane of the stair and the circular trajectory of P_2 around the centre point H_2. The distance between P_M and the level ground is denoted by H_M.

With respect to the coordinate system defined in Figure 14, the position vector of H_2 is

$$\boldsymbol{P}_{H_2} = [D\cos\alpha,\ 0,\ D\sin\alpha]^T \tag{11}$$

The trajectory circle of P_2 can be expressed as

$$(x - D\cos\alpha)^2 + (z - D\sin\alpha)^2 = L_2^2 \tag{12}$$

Substituting $x = L$ (the line projected by the vertical plane of the stair) into Eq. 12, we get

$$H_M = \sqrt{L_2^2 - (L - D\cos\alpha)^2} + D\sin\alpha + h_0 \tag{13}$$

The $H_M(\alpha)$ function is monotonically increasing in the range of $\alpha \in [0,\ \pi/2]$. In other words, the larger the value of α, the larger the stair that the robot can climb. In addition, it can be seen from Figure 15 that joint H_2 is higher for the robot with pitching capability, which is helpful to create a more efficient angle between leg 2 and the horizontal surface of the stair, thus avoiding foot slipping and providing a greater friction force to push the robot forward.

As shown in Figure 16, when the front half of the trunk is pitching upwards, the COG of the robot will move backwards by a distance of Δd, and will be lifted upwards by a distance of Δh along the z axis. From Eq. 10, we obtain

$$\Delta d = \frac{d_0\,(1 - \cos\alpha)}{2} = \frac{d_0 \sin\,(\alpha/2)^2}{2} \tag{14a}$$

$$\Delta h = \frac{d_0 \sin\alpha}{2} \tag{14b}$$

In Step 3, the support polygon of the quadruped robot is $\triangle P_1P_3P_4$, as shown in Figure 16(a), where D represents the distance between the axis of joint H_i and the y axis, S denotes the distance between the foothold P_i and the xz plane, $\triangle l$ stands for the distance between the foothold P_1 and the yz plane. To avoid interference between leg 1 and leg 2, $\triangle l$ must be greater than zero. D and S are constant during the gait cycle. d_{ij} represents the distance between the G_0 (projected on xy) plane and P_iP_j. The SSM will be equal to either d_{13} or d_{14}, whichever is smallest, as described by the following equation:

$$\text{SSM} = \min\,(d_{13},\ d_{14}) \tag{15}$$

where

$$d_{13} = \frac{\left|S^2 + (D - \triangle d)(\triangle d - \triangle l)\right|}{\sqrt{4S^2 + (D - \triangle l)^2}} \tag{16a}$$

$$d_{14} = \frac{\left|S^2 + (D + \triangle d)(\triangle d - \triangle l)\right|}{\sqrt{4S^2 + (D - \triangle l)^2}} \tag{16b}$$

Journal of Mechanisms and Robotics. Received December 01, 2021;
Accepted manuscript posted April 17, 2022. doi:10.1115/1.4054408

It is easily seen from Figure 16 that when the front half of the trunk is pitching upwards, d_{14} increases, while d_{13} decreases. Accordingly, the stability margin reaches its maximum value when d_{13} is equal to d_{14}. In this case, Δd can be obtained by

$$\Delta d = \frac{1}{2}\left(\frac{D\left(\sin\phi_3 - \sin\phi_4\right)}{\sin\phi_3 + \sin\phi_4} + \Delta l\right) \tag{17}$$

where $\phi_3 = \arctan\left(\frac{2S}{D-\Delta l}\right)$, and $\phi_4 = \arctan\left(\frac{2S}{D+\Delta l}\right)$. ϕ_3 and ϕ_4 represent $\angle P_1P_3P_4$ and $\angle P_1P_4P_3$, respectively.

According to Eqs. 14(a) and 17, the pitching angle corresponding to the maximum SSM can be written as

$$\alpha_{max} = \arccos\left(1 - \frac{1}{d_0}\left(\frac{M-N}{M+N} + \Delta l\right)\right) \tag{18}$$

where

$$M = \sqrt{4S^2 + (D+\Delta l)^2}$$
$$N = \sqrt{4S^2 + (D-\Delta l)^2}$$

Thus the robot with the pitching trunk retains the ability to conduct Step 3 of the STC gait with the highest degree of stability.

The above case describes the robot's postural stability for $\alpha > 0$. We further look into the $\alpha < 0$ case. In Step 12, legs 2 and 4 stand on the stair, and Leg 1 stands on the ground, while leg 3 is in the swing phase and will be placed on the stair before the next step. The simplified model of the biomimetic quadruped robot in Step 12 is depicted in Figure 17(a), where ΔH represents the distance between the geometrical center o and the horizontal plane of the stair, H denotes the height of the stair, β stands for the angle made by the horizontal plane and the rear half of the trunk, and l_{pi} represents the distance between the foothold P_i and the vertical plane of the stair. A similar robot with a rigid trunk is also depicted in Figure 17(b) for comparison. For Step 12 of the STC gait, the position vector of G_{F2} can be expressed as

$$\boldsymbol{P}_{G_{F2}} = d_0\left[\cos(\beta-\alpha)),\ 0, \sin(\beta-\alpha)\right]^T \tag{19}$$

The position vector of G_{R2} is

$$\boldsymbol{P}_{G_{R2}} = -d_0\left[\cos(\beta)),\ 0, \sin(\beta)\right]^T \tag{20}$$

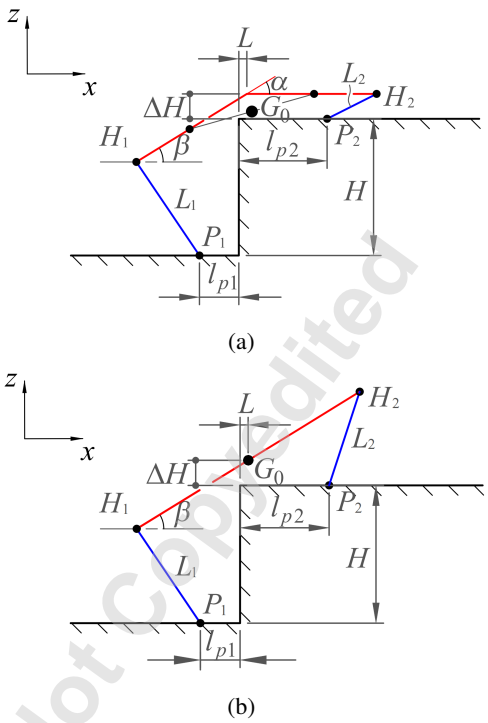

Fig. 17: Simplified models of the robot (Step 12) projected on the xz plane: (a) with a pitching trunk, and (b) with a rigid trunk.

Thus the position vector of G_0 is obtained by

$$\boldsymbol{P}_{G_0} = \frac{d_0}{2}\left[\left(\cos(\beta-\alpha) - \cos\beta\right),\ 0,\ \left(\sin(\beta-\alpha) - \sin\beta\right)\right]^T \tag{21}$$

After the pitching motion of Step 8, the front half of the trunk is nearly parallel to the ground, and the distance between the joint H_i ($i = 2,\ 4$) and the horizontal plane of the stair is reduced, which means that the robot can extend its front legs down toward the stair more easily, as shown in Figure 18(a). In contrast, a robot with a rigid trunk demonstrates inefficient leg positioning with its front legs extended a little awkwardly downwards, as shown in Figure 18(b). Figure 19 shows a top view of the simplified model in Step 12. It can be seen that the geometrical center o and the GOC of the robot have crossed the vertical face of the stair. Due to the pitching motion, the distance between G_0 and the vertical face of the stair is larger than the distance between the geometrical center o and the vertical surface of the stair. As the COG of the rigid trunk is identical with the geometrical center o, and P_1P_4 is the precarious edge of the support triangle $\triangle P_1P_2P_4$, we can conclude that the pitching motion im-

Journal of Mechanisms and Robotics. Received December 01, 2021;
Accepted manuscript posted April 17, 2022. doi:10.1115/1.4054408

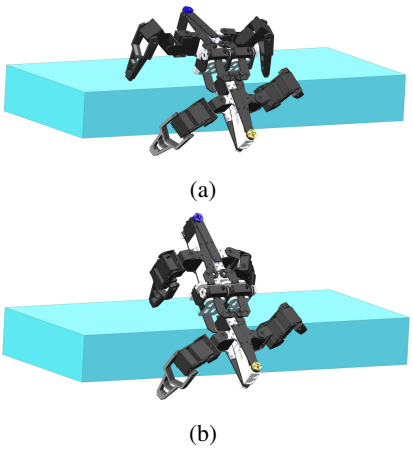

Fig. 18: The robot in Step 12: (a) with a pitching trunk, and (b) with a rigid trunk.

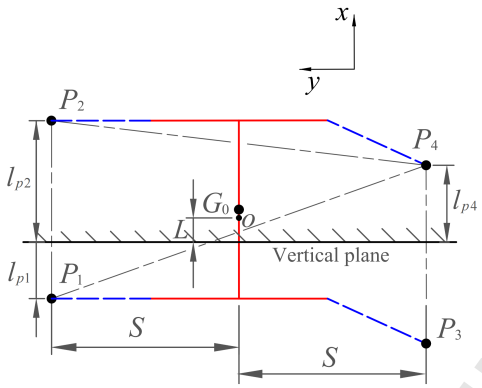

Fig. 19: The top view of the simplified model of the biomimetic quadruped robot in Step 12.

proves the stability of the robot when climbing stairs, see Figure 19.

In summary, as the pitching motion enlarges the leg workspace, the metamorphic trunk robot design can overcome higher obstacles , as compared to the one with a rigid trunk. Besides, in comparison to its rigid counterpart, the trunk with pitching ability not only improves the stability of the proposed robot when climbing stairs, but also allows the legs to realise more efficient poses that avoid slippage and provide more propulsion.

5.4 Locomoting over special terrains

The biomimetic quadruped robot is able to change its configuration to befit different terrains. In this section, two examples are included to demonstrate the enhanced

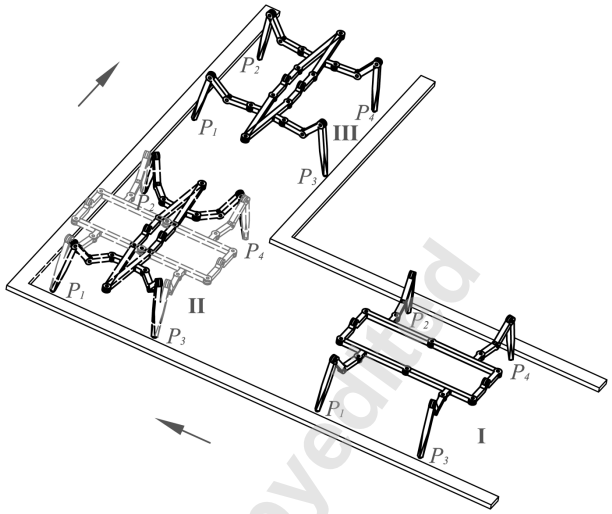

Fig. 20: Making a quarter turn by changing the biomimetic configuration.

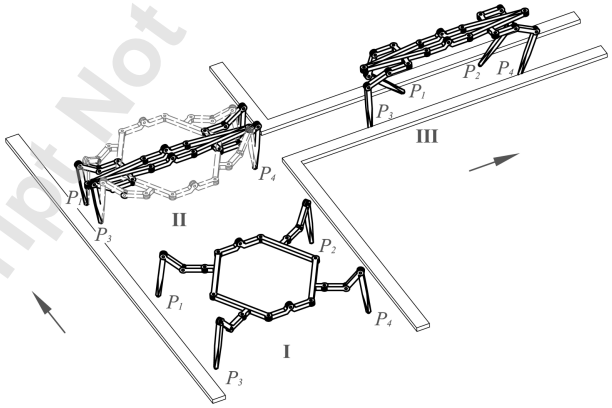

Fig. 21: Passing through a narrow path by changing the biomimetic configuration.

adaptability offered by the reconfigurability of the robot.

5.4.1 *Right-angled bend*

Right-angle corners are ubiquitous in the physical world. After a quarter turn, the moving direction of the robot will be shifted by 90 degrees. Most traditional legged robots adopt the spinning gait to adjust the direction of their forward movement. By contrast, the bionic metamorphic robot can change its moving direction by switching its configuration, so as to swiftly make a turn, as shown in Figure 20. It is noted that the front (legs 1 and 2) and rear legs (legs 3 and 4) become the left and right ones after the reconfiguring motion. Besides, in conjunction with the link rotation of the trunk, each leg and

Journal of Mechanisms and Robotics. Received December 01, 2021;
Accepted manuscript posted April 17, 2022. doi:10.1115/1.4054408

its workspace rotate by approximately 90 degrees [25], which means the legs have the same kinematic properties in the new direction.

5.4.2 *Narrow path*

Narrow paths can be frequently encountered by legged robots, and whether a robot can traverse such an environment depends mostly on its size. Most traditional legged robots have bodies of fixed size, and cannot go through narrow paths smaller than their lateral dimensions. The metamorphic quadruped robot can take advantage of the reconfiguration of the trunk to reduce its lateral size for traversing such narrow passages, as shown in Figure 21. To be more specific, the robot first needs to shrink its trunk into the configuration of mode 3. To minimize the width of the robot, the first joint of each leg also rotates about a certain angle, so that the four legs can be as close to the trunk as possible. When passing through the narrow path, the robot cannot move in a standard mode 3 way, in which the movement of the foothold of each leg is mainly realised by the rotation of the first joint. As mentioned in Section 4.1, mode 4 of the biomimetic quadruped robot is also highly effective in terms of navigating narrow paths.

6 PROTOTYPE AND EXPERIMENTS

A prototype of the biomimetic metamorphic robot was developed, upon which experiments were conducted to validate its enhanced locomotivity, as well as the proposed gaits and locomotion strategies.

6.1 Prototype of the biomimetic quadruped robot

The biomimetic quadruped robot has four identical legs, which are symmetrically-arranged around the trunk and fixed on links BC, CD, FG, and GH, respectively, as shown in Figure 22. Each leg is a 3-bar serial mechanism. The robot has 16 motors, four of which are used to drive the trunk, and twelve to drive its four legs, as stated in Section 4.1. The pin-hole component introduced in Section 4.2 avoids the loss of control at singular positions, thus reducing the use of one motor. The dimensional parameters of the prototype are listed in Table 2. The mechanical components of the prototype are mostly sheet metal components and plastic parts manufactured using a 3D printer. Considerable effort was made to avoid physical interference and simplify component replacement, such as the controller, the motors, the wires, the broken links, and the damaged leg parts. As the robot is highly reconfigurable, the interference issue is an important one to consider. In addition, easy part replacement is essential for experiments on challenging terrains, in case components are damaged during risky maneuvers.

Table 2: Structure parameters of the prototype.

Parameters	l_1	l_2	d_1	d_2	s_1	s_2	s_3
Lengths[mm]	140	50	40	90	46	54	110

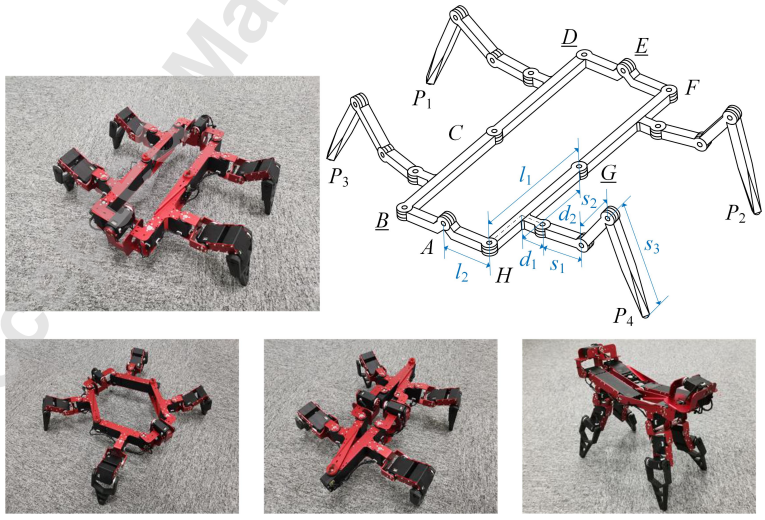

Fig. 22: Prototype of the biomimetic quadruped robot.

Journal of Mechanisms and Robotics. Received December 01, 2021;
Accepted manuscript posted April 17, 2022. doi:10.1115/1.4054408

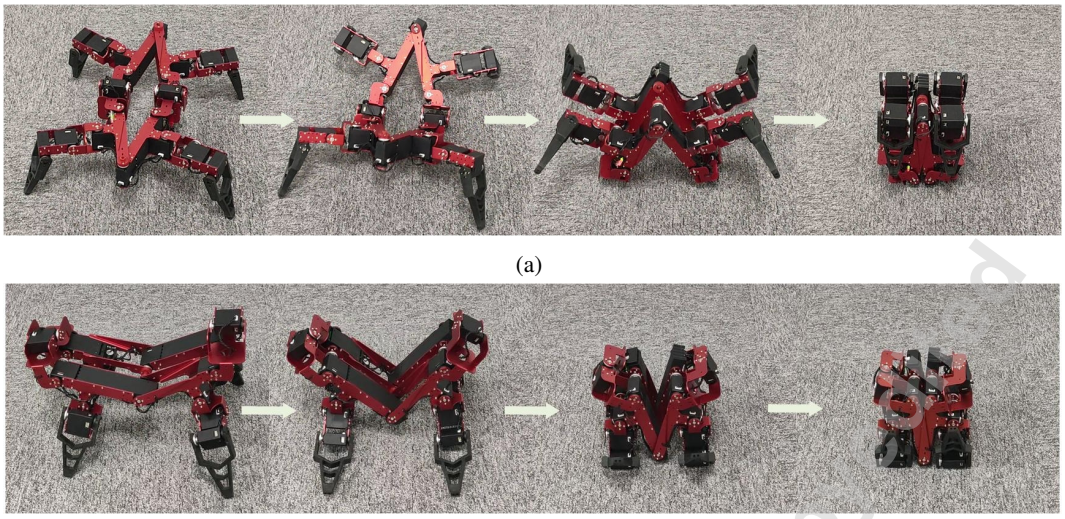

(a)

(b)

Fig. 23: The robot packaging from: (a) mode 3, and (b) mode 4 (see video).

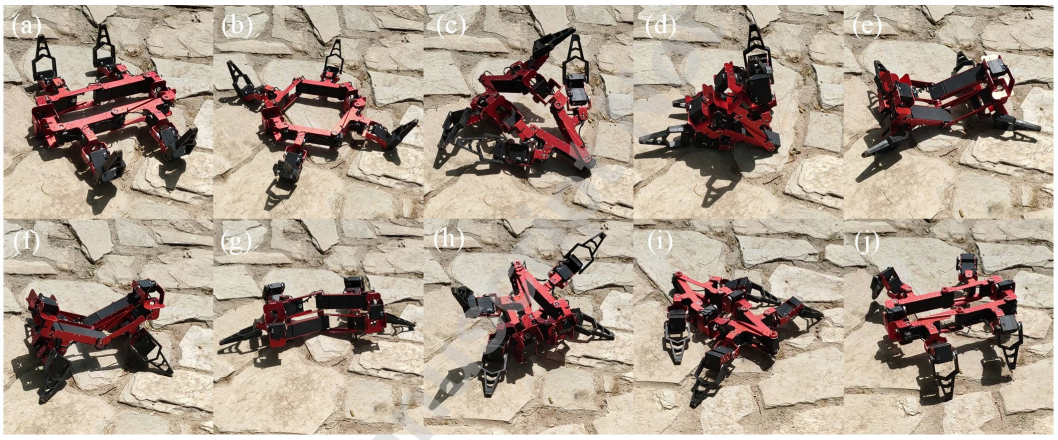

Fig. 24: Self recovery of the biomimetic quadruped robot (see video).

6.2 Experiments

In this section, the results of the experiments conducted on the robot are presented. We tested the robot when locomoting over different terrains, performing various maneuvers which included packaging, self recovery from the supine position, climbing over obstacles, and demonstrating the FSP gait in which the robot can make a fast turn by integrating a twist motion. A video offering additional details about the robot can be accessed at: https://www.youtube.com/watch?v=GFQwaioO3Ug.

6.2.1 Packaging

By virtue of the inclusion of a metamorphic trunk, the robot is able to be fully folded into a cuboid ($150 \times 150 \times 175$ mm), which significantly reduces the space occupied by the robot and makes it easier to carry. As analyzed in Section 4.2, the robot can package from both modes 3 and 4. Figure 23 displays the results of the packaging experiments, which demonstrates that the robot can be automatically folded from these two routes, without any collision.

6.2.2 Self recovery

The risk of overturning caused by external disturbances is unavoidable for quadruped robots. The metamorphic trunk endows the robot with the capability of recovering from a supine or side-lying pose. Figure 24 demonstrates the result of the self-recovery experiment,

Journal of Mechanisms and Robotics. Received December 01, 2021;
Accepted manuscript posted April 17, 2022. doi:10.1115/1.4054408

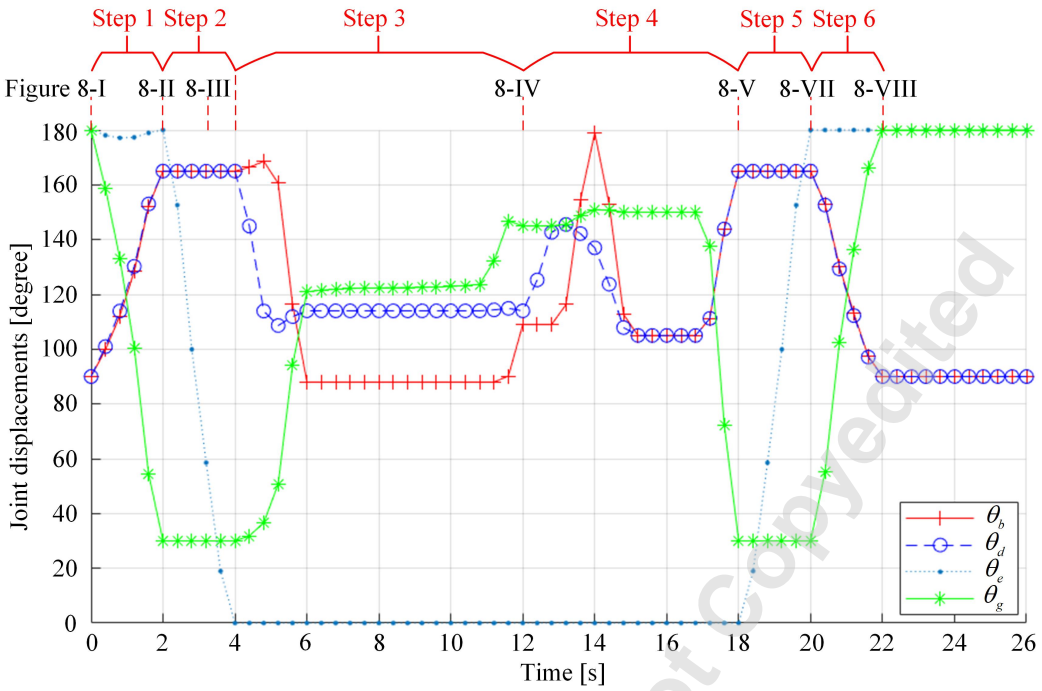

Fig. 25: Joint displacements of the active joints of the trunk when performing self recovery actions.

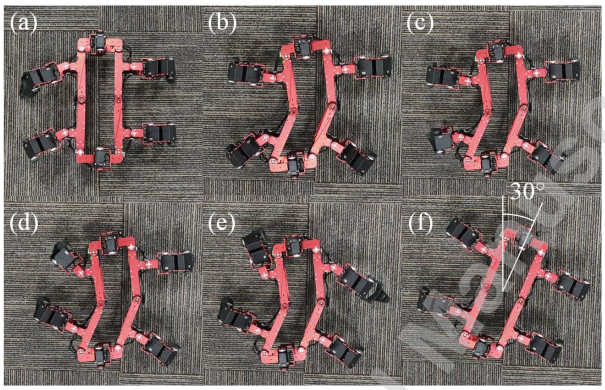

Fig. 26: The robot executing the FSP gait (see video).

which shows that the robot successfully recovered its standing pose with the proposed strategy.

Figure 25 shows the displacement variations of the active joints of the trunk when executing self recovery sequences. Here the angular displacements of the active joints B, D, E, and G are denoted as θ_b, θ_d, θ_e, and θ_g, which are defined as the angles of $\angle ABC$, $\angle CDE$, $\angle DEF$, and $\angle FGH$, respectively. The whole self recovery process takes 22 seconds. Between 6s and 11s, the configuration of the trunk does not change, and the robot moves its legs to support itself and maintain balance. At 2-4s and 18-20s, the trunk rotates around the joints A and E. In order to keep the axes of joints A and E collinear, the following must be satisfied

$$\theta_b + \theta_d + \theta_g = 360^\circ \tag{22a}$$
$$\theta_b = \theta_d \tag{22b}$$

When performing the self-recovery actions, each motor is operated in position-control mode, thereby enabling the realisation of a pre-planned position trajectory. Compared to some existing, dynamically-controlled methods, the proposed static strategy that is based on a controllable trunk exhibits higher repeatability, as well as a higher success rate of execution in different environments.

6.2.3 *FSP gait*

By including the twist motion into the traditional spinning gait, the FSP gait is expected to achieve fast turning. Figure 26 shows that the robot is able to rotate stably by 30° from the initial pose through only four steps.

6.2.4 *STC gait*

With mode 3, the robot is able to pitch upwards or downwards, and this endows the robot with improved lev-

Journal of Mechanisms and Robotics. Received December 01, 2021;
Accepted manuscript posted April 17, 2022. doi:10.1115/1.4054408

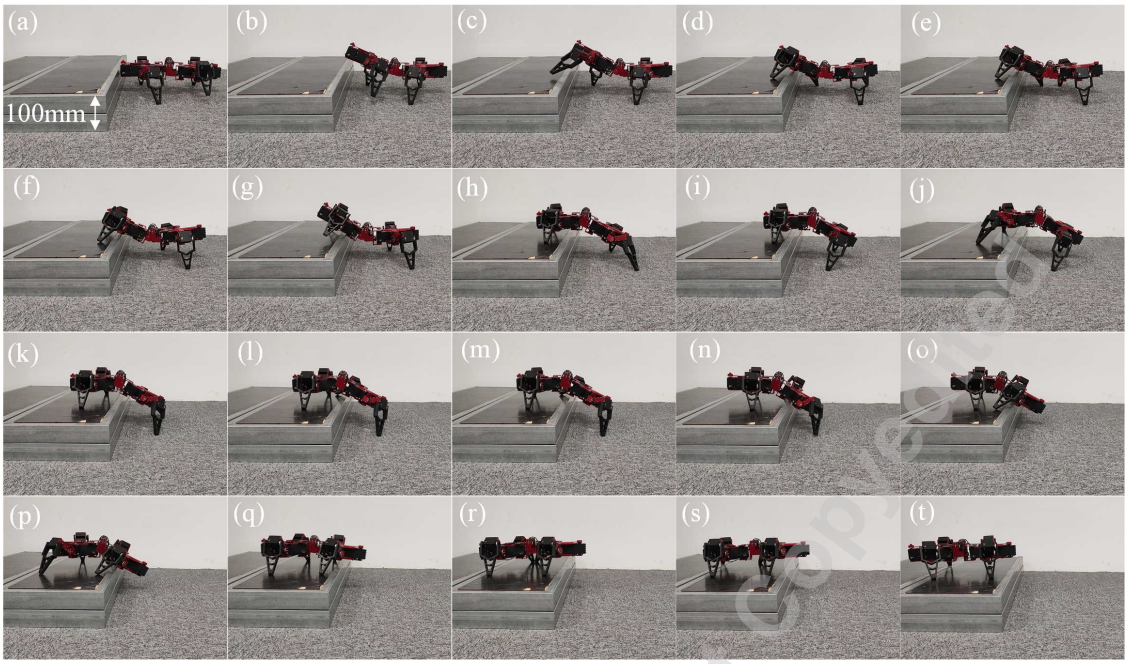

Fig. 27: The robot executing the STC gait (see video).

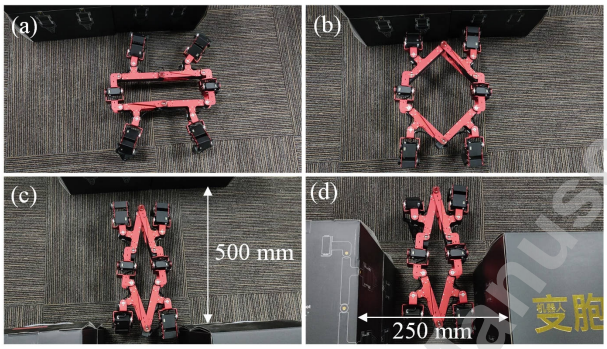

Fig. 28: The robot passing through right-angled bend and narrow path (see video).

els of stability, in comparison to its rigid-trunk counterpart, as analyzed in Section 5.3.2. The experimental results demonstrate that the robot is able to crawl over an obstacle of 100mm in height when using the STC gait, as shown in Figure 27.

6.2.5 *Quarter turn & crawling through the narrow path*

By transforming from mode 1 to mode 3, the robot is able to make a faster quarter turn than those achieved by the spinning gaits. By shrinking its total size in mode 3, the robot is able to crawl through a narrow path of 250mm in width, as shown in Figure 28.

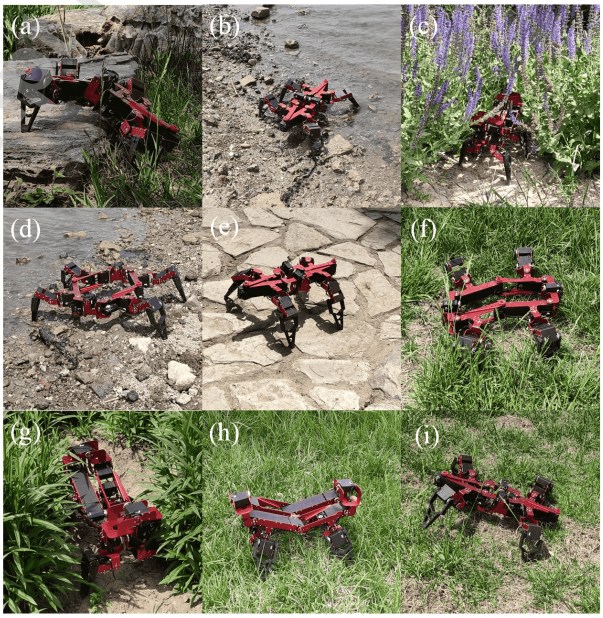

Fig. 29: The robot crawling over various terrains (see video).

6.2.6 *Crawling over a variety of surfaces in outdoor experiments*

In addition to indoor experiments, we also tested the robot outdoors on various real-world terrains, some of which even included relatively challenging obstacles, as can be seen in Figure 29 and in the video attachment. The robot successfully performed self-recovery and executed different gaits on a grass surface. The robot also crawled successfully over rough sandy surfaces, narrow paths and other unstructured environments.

7 CONCLUSIONS

In this paper, we presented a novel, highly reconfigurable quadruped robot that can change its working modes according to different terrains. A metamorphic, single-loop linkage was designed as the trunk of the proposed robot, whose configuration space and transformation routes were analyzed and illustrated. The integrated design of the quadruped robot and metamorphic mechanism endows the robot with the ability to realise multiple types of mimicry, and endows it with a superior ability in terms of engaging with different terrains, thus outperforming our previously designed robot [20].

To the best of the authors' knowledge, the FSP and STC gaits are proposed herein for the first time to demonstrate the maneuverability enhancements provided by the twisting and pitching abilities, respectively. The inclusion of the metamorphic mechanism enables the robot to recover from a supine position, especially for the sprawling-type modes that possess higher levels of intrinsic stability, although they make it more challenging for the robot to roll over due to the increased support polygon dimensions. By utilizing its reconfigurability, the robot can significantly reduce its width to pass through narrow spaces, and even package itself for easy transportation.

In addition, this work also provides insight into the design of metamorphic robots, and is expected to help researchers in related fields for designing multi-functional robots based on metamorphic mechanisms.

In this paper, we mainly focus on the design of a multi-mimicry quadruped robot, in addition to contriving gaits that account for the effects of the body's motion, while also analysing additional functions provided by the metamorphic trunk. Other aspects, such as robot-environment interaction and control algorithms combined with complex sensing, will be considered in future studies.

REFERENCES

[1] Biewener, A. A., 2003, *Animal Locomotion* Oxford University Press.

[2] Kau, N., Schultz, A., Ferrante, N., and Slade, P., 2019, "Stanford Doggo: An open-source, quasi-direct-drive quadruped," In IEEE International Conference on Robotics and Automation, pp. 6309–6315.

[3] Katz, B., Carlo, J. D., and Kim, S., 2019, "Mini Cheetah: A platform for pushing the limits of dynamic quadruped control," In IEEE International Conference on Robotics and Automation, pp. 6295–6301.

[4] Hutter, M., Gehring, C., Lauber, A., Gunther, F., Bellicoso, C. D., Tsounis, V., Fankhauser, P., Diethelm, R., Bachmann, S., Bloesch, M., Kolvenbach, H., Bjelonic, M., Isler, L., and Meyer, K., 2017, "ANYmal - toward legged robots for harsh environments," *Advanced Robotics,* **31**(17), pp. 918–931.

[5] Kolter, J. Z., and Ng, A. Y., 2011, "The Stanford LittleDog: A learning and rapid replanning approach to quadruped locomotion," *The International Journal of Robotics Research,* **30**(2), pp. 150–174.

[6] Raibert, M., Blankespoor, K., Nelson, G., and Playter, R., 2008, "Bigdog, the rough-terrain quadruped robot," *IFAC Proceedings Volumes,* **41**(2), pp. 10822–10825.

[7] Havoutis, I., Ortiz, J., Bazeille, S., Barasuol, V., Semini, C., and Caldwell, D. G., 2013, "Onboard perception-based trotting and crawling with the hydraulic quadruped robot (HyQ)," In 2013 IEEE/RSJ International Conference on Intelligent Robots and Systems, pp. 6052–6057.

[8] Fukuoka, Y., Kimura, H., Hada, Y., and Takase, K., 2003, "Adaptive dynamic walking of a quadruped robot 'Tekken' on irregular terrain using a neural system model," In IEEE International Conference on Robotics and Automation, Vol. 2, pp. 2037–2042.

[9] Seok, S., Wang, A., Chuah, M. Y., Otten, D., Lang, J., and Kim, S., 2013, "Design principles for highly efficient quadrupeds and implementation on the mit cheetah robot," In IEEE International Conference on Robotics and Automation, pp. 3307–3312.

[10] Hildebrand, M., 1959, "Motions of the Running Cheetah and Horse," *Journal of Mammalogy,* **40**(4), 11, pp. 481–495.

[11] Akhlaq, A., Ahmad, J., and Umber, A., 2014, "Biologically inspired self-reconfigurable hexapod with adaptive locomotion," In IEEE International Power Electronics and Motion Control Conference and Ex-

position, pp. 432–438.

[12] Ritzmann, R. E., Quinn, R. D., and Fischer, M. S., 2004, "Convergent evolution and locomotion through complex terrain by insects, vertebrates and robots," *Arthropod Structure & Development,* **33**(3), pp. 361–379.

[13] Eckert, P., Spröwitz, A., Witte, H., and Ijspeert, A. J., 2015, "Comparing the effect of different spine and leg designs for a small bounding quadruped robot," In IEEE International Conference on Robotics and Automation, pp. 3128–3133.

[14] Kani, M. H. H., Derafshian, M., Bidgoly, H. J., and Ahmadabadi, M. N., 2011, "Effect of flexible spine on stability of a passive quadruped robot: Experimental results," In IEEE International Conference on Robotics and Biomimetics, pp. 2793–2798.

[15] Fisher, C., Shield, S., and Patel, A., 2017, "The effect of spine morphology on rapid acceleration in quadruped robots," In IEEE/RSJ International Conference on Intelligent Robots and Systems, pp. 2121–2127.

[16] Liu, Q., Bao, Y., Yu, W., Zhang, J., Li, C., and Xie, X., 2019, "Mechanism of spine motion about contact time in quadruped running," *Chinese Journal of Mechanical Engineering,* **32**(18), pp. 1–8.

[17] Yesilevskiy, Y., Yang, W., and Remy, C. D., 2018, "Spine morphology and energetics: how principles from nature apply to robotics," *Bioinspiration & Biomimetics,* **13**(3), mar, p. 036002.

[18] Chai, X., Kang, X., Gan, D., Yu, H., and Dai, J. S., 2021, "Six novel 6r metamorphic mechanisms induced from three-series-connected bennett linkages that vary among classical linkages," *Mechanism and Machine Theory,* **156**, p. 104133.

[19] Zhang, C., and Dai, J. S., 2018, "Continuous static gait with twisting trunk of a metamorphic quadruped robot," *Mechanical Sciences,* **9**(1), pp. 1–14.

[20] Zhang, C., and Dai, J., 2018, "Trot gait with twisting trunk of a metamorphic quadruped robot," *Journal of Bionic Engineering,* **15**, p. 971–981.

[21] Zhang, C., Zhang, C., Dai, J. S., and Qi, P., 2019, "Stability margin of a metamorphic quadruped robot with a twisting trunk," *Journal of Mechanisms and Robotics,* **11**(6), p. 064501.

[22] Spyrakos-Papastavridis, E., and Dai, J. S., 2020, "A model-free solution for stable balancing and locomotion of floating-base legged systems," In IEEE/RSJ International Conference on Intelligent Robots and Systems (IROS), pp. 3816–3822.

[23] Spyrakos-Papastavridis, E., Childs, P. R. N., and Dai, J. S., 2020, "Passivity preservation for variable impedance control of compliant robots," *IEEE/ASME Transactions on Mechatronics,* **25**(5), pp. 2342–2353.

[24] Spyrakos-Papastavridis, E., and Dai, J. S., 2021, "Minimally model-based trajectory tracking and variable impedance control of flexible-joint robots," *IEEE Transactions on Industrial Electronics,* **68**(7), pp. 6031–6041.

[25] Tang, Z., Qi, P., and Dai, J. S., 2017, "Mechanism design of a biomimetic quadruped robot," *Industrial Robot: An International Journal,* **44**(4), pp. 512–520.

[26] Zhong, Y., Wang, R., Feng, H., and Chen, Y., 2019, "Analysis and research of quadruped robot's legs: A comprehensive review," *International Journal of Advanced Robotic Systems,* **16**(3), pp. 1–15.

[27] Cordes, S., Berns, K., Eberl, M., Ilg, W., and Buhrle, P., 1997, "On the design of a four-legged walking machine," In IEEE International Conference on Advanced Robotics, pp. 65–70.

[28] Xu, K., Ma, H., Chen, J., Zhang, W., Deng, H., and Ding, X., 2018, "Design and analysis of a metamorphic quadruped robot," In International Conference on Reconfigurable Mechanisms and Robots, pp. 1–7.

[29] Castano, A., Shen, W., and Will, P., 2000, "CONRO: towards deployable robots with inter-robots metamorphic capabilities," *Autonomous Robots,* **8**, pp. 309–324.

[30] Ozyalcin, K., Akay, I. H., Ozturk, Y., Mengus, B., Ozakyol, H., and Bingul, Z., 2018, "New design and development of reconfigurable-hybrid hexapod robot," In IECON 2018 - 44th Annual Conference of the IEEE Industrial Electronics Society, pp. 2583–2588.

[31] Jakimovski, B., and Maehle, E., 2010, "In situ self-reconfiguration of hexapod robot oscar using biologically inspired approaches," In *Climbing and Walking Robots*, B. Miripour, ed. IntechOpen, Rijeka, ch. 19, pp. 311–332.

[32] Ding, X., Zheng, Y., and Xu, K., 2017, "Wheel-legged hexapod robots: a multifunctional mobile manipulating platform," *Chinese Journal of Mechanical Engineering,* **30**(1), p. 3–6.

[33] Gao, W., Huo, K., Seehra, J. S., Ramani, K., and Cipra, R. J., 2014, "Hexamorph: A reconfigurable and foldable hexapod robot inspired by origami," In IEEE/RSJ International Conference on Intelligent Robots and Systems, pp. 4598–4604.

[34] Wu, J., Yang, H., Li, R., Ruan, Q., Yan, S., and an Yao, Y., 2021, "Design and analysis of a novel octopod platform with a reconfigurable

trunk," *Mechanism and Machine Theory,* **156**, p. 104134.

[35] Zhao, J.-S., Wang, J.-Y., Chu, F., Feng, Z.-J., and Dai, J. S., 2011, "Structure synthesis and statics analysis of a foldable stair," *Mechanism and Machine Theory,* **46**(7), pp. 998–1015.

[36] Dai, J. S., and Rees Jones, J., 1999, "Mobility in metamorphic mechanisms of foldable/erectable kinds," *Journal of Mechanical Design,* **121**(3), 09, pp. 375–382.

[37] Zhao, C., Guo, H., Liu, R., Deng, Z., Li, B., and Tian, J., 2019, "Actuation distribution and workspace analysis of a novel 3(3RRlS) metamorphic serial-parallel manipulator for grasping space non-cooperative targets," *Mechanism and Machine Theory,* **139**, pp. 424–442.

[38] Carroll, D. W., Magleby, S. P., Howell, L. L., Todd, R. H., and Lusk, C. P., 2005, "Simplified manufacturing through a metamorphic process for compliant ortho-planar mechanisms," ASME International Mechanical Engineering Congress and Exposition, Design Engineering, Parts A and B, pp. 389–399.

[39] Li, S., and Dai, J. S., 2012, "Structure synthesis of single-driven metamorphic mechanisms based on the augmented Assur groups," *Journal of Mechanisms and Robotics,* **4**(3), 05 031004.

[40] Jia, G., Huang, H., Wang, S., and Li, B., 2021, "Type synthesis of plane-symmetric deployable grasping parallel mechanisms using constraint force parallelogram law," *Mechanism and Machine Theory,* **161**, p. 104330.

[41] Aten, Q. T., Jensen, B. D., Burnett, S. H., and Howell, L. L., 2014, "A self-reconfiguring metamorphic nanoinjector for injection into mouse zygotes," *Review of Scientific Instruments,* **85**(5), p. 055005.

[42] Zhang, K., and Dai, J. S., 2014, "A Kirigami-inspired 8R linkage and its evolved overconstrained 6r linkages with the rotational symmetry of order two," *Journal of Mechanisms and Robotics,* **6**(2), 03 021007.

[43] Gan, D., Dai, J. S., and Liao, Q., 2009, "Mobility change in two types of metamorphic parallel mechanisms," *Journal of Mechanisms and Robotics,* **1**(4), 09 041007.

[44] Tang, Z., and Dai, J. S., 2018, "Bifurcated configurations and their variations of an 8-bar linkage derived from an 8-kaleidocycle," *Mechanism and Machine Theory,* **121**, pp. 745–754.

[45] López-Custodio, P. C., Dai, J. S., and Rico, J. M., 2018, "Branch reconfiguration of bricard linkages based on toroids intersections: Plane-symmetric case," *Journal of Mechanisms and Robotics,* **10**(3), 03 031002.

[46] López-Custodio, P. C., and Dai, J. S., 2019, "Design of a variable-mobility linkage using the Bohemian Dome," *Journal of Mechanical Design,* **141**(9), 04 092303.

[47] Kumar, P., and Pellegrino, S., 2000, "Computation of kinematic paths and bifurcation points," *International Journal of Solids and Structures,* **37**(46), pp. 7003–7027.

[48] Chen, Y., You, Z., and Tarnai, T., 2005, "Threefold-symmetric bricard linkages for deployable structures," *International Journal of Solids and Structures,* **42**(8), pp. 2287–2301.

[49] He, X., Kong, X., Chablat, D., Caro, S., and Hao, G., 2014, "Kinematic analysis of a single-loop reconfigurable 7R mechanism with multiple operation modes," *Robotica,* **32**(7), pp. 1171–1188.

[50] Kong, X., and Pfurner, M., 2015, "Type synthesis and reconfiguration analysis of a class of variable-DOF single-loop mechanisms," *Mechanism and Machine Theory,* **85**, pp. 116–128.

[51] Rico, J., Gallardo, J., and Duffy, J., 1999, "Screw theory and higher order kinematic analysis of open serial and closed chains," *Mechanism and Machine Theory,* **34**(4), pp. 559–586.

[52] Müller, A., 2014, "Higher derivatives of the kinematic mapping and some applications," *Mechanism and Machine Theory,* **76**, pp. 70–85.

[53] López-Custodio, P., Rico, J., Cervantes-Sánchez, J., Pérez-Soto, G., and Díez-Martínez, C., 2017, "Verification of the higher order kinematic analyses equations," *European Journal of Mechanics-A/Solids,* **61**, pp. 198–215.

[54] Kang, X., Feng, H., Dai, J. S., and Yu, H., 2020, "High-order based revelation of bifurcation of novel Schatz-inspired metamorphic mechanisms using screw theory," *Mechanism and Machine Theory,* **152**, p. 103931.

[55] Saab, W., Racioppo, P., and Ben-Tzvi, P., 2019, "A review of coupling mechanism designs for modular reconfigurable robots," *Robotica,* **37**(2), p. 378–403.

[56] Robertson, M. A., Murakami, M., Felt, W., and Paik, J., 2019, "A compact modular soft surface with reconfigurable shape and stiffness," *IEEE/ASME Transactions on Mechatronics,* **24**(1), pp. 16–24.

[57] Yao, M., Belke, C. H., Cui, H., and Paik, J., 2019, "A reconfiguration strategy for modular robots using origami folding," *The International Journal of Robotics Research,* **38**(1), pp. 73–89.

[58] Belke, C. H., and Paik, J., 2017, "Mori: A modular origami robot," *IEEE/ASME Transactions on*

Mechatronics, **22**(5), pp. 2153–2164.

[59] Gandhi, N., Saldaña, D., Kumar, V., and Phan, L. T. X., 2020, "Self-reconfiguration in response to faults in modular aerial systems," *IEEE Robotics and Automation Letters,* **5**(2), pp. 2522–2529.

[60] Long, J. A., and Gordon, M. S., 2004, "The greatest step in vertebrate history: a paleobiological review of the fish-tetrapod transition," *Physiological and biochemical zoology,* **77**(5), pp. 700–719.

[61] Hall, E. R., 1946, "The principles of classification and a classification of mammals," *Journal of Mammalogy,* **27**(3), pp. 287–288.

[62] Taylor, E. N., Diele-Viegas, L. M., Gangloff, E. J., Hall, J. M., Halpern, B., Massey, M. D., Rödder, D., Rollinson, N., Spears, S., Sun, B.-j., and Telemeco, R. S., 2021, "The thermal ecology and physiology of reptiles and amphibians: A user's guide," *Journal of Experimental Zoology Part A: Ecological and Integrative Physiology,* **335**(1), pp. 13–44.

[63] Basset, Y., Cizek, L., Cuénoud, P., Didham, R. K., Guilhaumon, F., Missa, O., Novotny, V., Ødegaard, F., Roslin, T., Schmidl, J., Tishechkin, A. K., Winchester, N. N., Roubik, D. W., Aberlenc, H.-P., Bail, J., Barrios, H., Bridle, J. R., Castaño-Meneses, G., Corbara, B., Curletti, G., Duarte da Rocha, W., De Bakker, D., Delabie, J. H. C., Dejean, A., Fagan, L. L., Floren, A., Kitching, R. L., Medianero, E., Miller, S. E., Gama de Oliveira, E., Orivel, J., Pollet, M., Rapp, M., Ribeiro, S. P., Roisin, Y., Schmidt, J. B., Sørensen, L., and Leponce, M., 2012, "Arthropod diversity in a tropical forest," *Science,* **338**(6113), pp. 1481–1484.

[64] Giribet, G., and Edgecombe, G. D., 2012, "Reevaluating the arthropod tree of life," *Annual Review of Entomology,* **57**(1), pp. 167–186.

[65] Polet, D. T., and Bertram, J. E. A., 2019, "An inelastic quadrupedal model discovers four-beat walking, two-beat running, and pseudo-elastic actuation as energetically optimal," *PLOS Computational Biology,* **15**, 11, pp. 1–29.

[66] Cruse, H., 1990, "What mechanisms coordinate leg movement in walking arthropods?," *Trends in Neurosciences,* **13**(1), pp. 15–21.

[67] Alexander, R. M., 1990, "Three uses for springs in legged locomotion," *The International Journal of Robotics Research,* **9**(2), pp. 53–61.

[68] Spagna, J. C., Goldman, D. I., Lin, P.-C., Koditschek, D. E., and Full, R. J., 2007, "Distributed mechanical feedback in arthropods and robots simplifies control of rapid running on challenging terrain," *Bioinspiration & Biomimetics,* **2**(1), pp. 9–18.

[69] Kwak, B., and Bae, J., 2018, "Locomotion of arthropods in aquatic environment and their applications in robotics," *Bioinspiration & Biomimetics,* **13**(4), p. 041002.

[70] Wang, K., Wu, X., Wang, Y., Li, B., Yuan, B., and Bai, S., 2021, "A novel 2-SUR 6-DOF parallel manipulator actuated by spherical motion generators," In IEEE/RSJ International Conference on Intelligent Robots and Systems (IROS), pp. 8022–8028.

[71] Wang, K., Wu, X., Wang, Y., Ding, J., and Bai, S., 2022, "Kinematics of a 6-DOF parallel manipulator with two limbs actuated by spherical motion generators," *Proceedings of the Institution of Mechanical Engineers, Part C: Journal of Mechanical Engineering Science,* **236**(6), pp. 2828–2846.

[72] Zhang, G., Du, J., and To, S., 2014, "Study of the workspace of a class of universal joints," *Mechanism and Machine Theory,* **73**, pp. 244–258.

[73] Galletti, C., and Fanghella, P., 2001, "Single-loop kinematotropic mechanisms," *Mechanism and Machine Theory,* **36**(6), pp. 743–761.

[74] Zhao, J.-S., Liu, X., Feng, Z.-J., and Dai, J. S., 2013, "Design of an Ackermann-type steering mechanism," *Proceedings of the Institution of Mechanical Engineers, Part C: Journal of Mechanical Engineering Science,* **227**(11), pp. 2549–2562.

[75] Tang, Z., and Dai, J. S., 2018, "Metamorphic mechanism and reconfiguration of a biomimetic quadruped robot," In ASME International Design Engineering Technical Conferences and Computers and Information in Engineering Conference, Volume 1A: 38th Computers and Information in Engineering Conference V01AT02A039.

[76] Zhang, X., Gong, J., and Yao, Y., 2016, "Effects of head and tail as swinging appendages on the dynamic walking performance of a quadruped robot," *Robotica,* **34**(12), pp. 2878–2891.

[77] Mastalli, C., Havoutis, I., Focchi, M., Caldwell, D. G., and Semini, C., 2020, "Motion planning for quadrupedal locomotion: Coupled planning, terrain mapping, and whole-body control," *IEEE Transactions on Robotics,* **36**(6), pp. 1635–1648.

[78] Miller, I. D., Cladera, F., Cowley, A., Shivakumar, S. S., Lee, E. S., Jarin-Lipschitz, L., Bhat, A., Rodrigues, N., Zhou, A., Cohen, A., Kulkarni, A., Laney, J., Taylor, C. J., and Kumar, V., 2020, "Mine tunnel exploration using multiple quadrupedal robots," *IEEE Robotics and Automation Letters,* **5**(2), pp. 2840–2847.

[79] Morgan, J., Magleby, S. P., and Howell, L. L., 2016, "An approach to designing Origami-adapted aerospace mechanisms," *Journal of Mechanical De-*

sign, **138**(5), 03 052301.

[80] Dai, J. S., Holland, N., and Kerr, D. R., 1995, "Finite twist mapping and its application to planar serial manipulators with revolute joints," *Proceedings of the Institution of Mechanical Engineers, Part C: Journal of Mechanical Engineering Science,* **209**(4), pp. 263–271.

[81] Kanehiro, F., Kaneko, K., Fujiwara, K., Harada, K., Kajita, S., Yokoi, K., Hirukawa, H., Akachi, K., and Isozumi, T., 2003, "The first humanoid robot that has the same size as a human and that can lie down and get up," In IEEE International Conference on Robotics and Automation, Vol. 2, pp. 1633–1639.

[82] Peng, S., Ding, X., Yang, F., and Xu, K., 2017, "Motion planning and implementation for the self-recovery of an overturned multi-legged robot," *Robotica,* **35**(5), pp. 1107–1120.

[83] Semini, C., Tsagarakis, N. G., Guglielmino, E., Focchi, M., Cannella, F., and Caldwell, D. G., 2011, "Design of HyQ – a hydraulically and electrically actuated quadruped robot," *Proceedings of the Institution of Mechanical Engineers, Part I: Journal of Systems and Control Engineering,* **225**(6), pp. 831–849.

[84] Niquille, S. C., 2019, "Regarding the pain of Spot-Mini: Or what a robot's struggle to learn reveals about the built environment," *Architectural Design,* **89**(1), pp. 84–91.

[85] Spyrakos-Papastavridis, E., Kashiri, N., Childs, P. R., and Tsagarakis, N. G., 2018, "Online impedance regulation techniques for compliant humanoid balancing," *Robotics and Autonomous Systems,* **104**, pp. 85–98.

[86] Spyrakos-Papastavridis, E., Kashiri, N., Lee, J., Tsagarakis, N. G., and Caldwell, D. G., 2015, "Online impedance parameter tuning for compliant biped balancing," In IEEE-RAS 15th International Conference on Humanoid Robots (Humanoids), pp. 210–216.

[87] Spyrakos-Papastavridis, E., and Dai, J. S., 2021, "Flexible-joint humanoid balancing augmentation via full-state feedback variable impedance control," *Journal of Mechanisms and Robotics,* **13**(2), 02 021014.

[88] Spyrakos-Papastavridis, E., Caldwell, D. G., and Tsagarakis, N. G., 2016, "Balance and impedance optimization control for compliant humanoid stepping," In 2016 IEEE/RSJ International Conference on Intelligent Robots and Systems (IROS), pp. 1349–1355.

[89] Yang, C., Yuan, K., Zhu, Q., Yu, W., and Li, Z., 2020, "Multi-expert learning of adaptive legged locomotion," *Science Robotics,* **5**(49), Dec, p. eabb2174.

[90] Messuri, D., and Klein, C., 1985, "Automatic body regulation for maintaining stability of a legged vehicle during rough-terrain locomotion," *IEEE Journal on Robotics and Automation,* **1**(3), pp. 132–141.

[91] Zhang, C.-D., and Song, S.-M., 1992, "Turning gaits of a quadrupedal walking machine," *Advanced Robotics,* **7**(2), pp. 121–157.

[92] González de Santos, P., Garcia, E., and Estremera, J., 2006, *Quadrupedal Locomotion: An Introduction to the Control of Four-legged Robots* Springer Science & Business Media, London.